Complementary aerosol mass spectrometry elucidates sources of wintertime sub-micron particle pollution in Fairbanks, Alaska, during ALPACA 2022

Amna Ijaz[1,2], Brice Temime-Roussel[1], Benjamin Chazeau[1], Sarah Albertin[3], Stephen R. Arnold[4], Brice Barret[5], Slimane Bekki[6], Natalie Brett[6], Meeta Cesler-Maloney[7], Elsa Dieudonne[8], Kayane K. Dingilian[9], Javier Fochesatto[10], Jingqiu Mao[7], Allison Moon[11], Joel Savarino[3], William Simpson[7], Rodney J. Weber[9], Kathy S. Law[6], Barbara D'Anna[1]

[1]Aix-Marseille Université, CNRS, LCE, Marseille, France
[2]Present Address: Atmospheric, Climate, & Earth Sciences Division, Pacific Northwest National Laboratory, Richland, Washington 99354, United States
[3]University of Grenoble Alpes, CNRS, IRD, Grenoble INP, INRAE, IGE, F-38000 Grenoble, France
[4]School of Earth and Environment, University of Leeds, Leeds, LS2 9JT, United Kingdom
[5]Laboratoire d'Aérologie, Université Toulouse III-Paul Sabatier, CNRS, Toulouse, France
[6]Sorbonne Université, UVSQ, CNRS, LATMOS-IPSL, Paris, France
[7]Department of Chemistry and Biochemistry and Geophysical Institute, University of Alaska, Fairbanks, AK, United States
[8]Laboratory of Physics and Chemistry of the Atmosphere, University of Littoral and Opal Coast, Dunkerque, France
[9]School of Earth and Atmospheric Sciences, Georgia Institute of Technology, Atlanta, Georgia 30332, United States
[10]Department of Atmospheric Sciences, University of Alaska, Fairbanks, AK, United States
[11]Department of Atmospheric Sciences, University of Washington, Seattle, Washington 98195, United States

Correspondence to: Barbara D'Anna (barbara.danna@univ-amu.fr) and Amna Ijaz (amna.ijaz@pnnl.gov)

Fairbanks, Alaska, is a sub-arctic city that frequently suffers from non-attainment of national air quality standards in the wintertime due to the coincidence of weak atmospheric dispersion and increased local

emissions. As part of the Alaskan Layered Pollution and Chemical Analysis (ALPACA) campaign, we deployed a Chemical Analysis of Aerosol Online (CHARON) inlet coupled with a proton transfer reaction - time of flight mass spectrometer (PTR-ToF MS) and an Aerodyne high-resolution aerosol mass spectrometer (AMS) to measure organic aerosol (OA) and NR-PM_1, respectively. We deployed Positive Matrix Factorisation (PMF) analysis for source identification of the NR-PM_1. The AMS analysis identified three primary factors: biomass burning, hydrocarbon-like, and cooking factors, which together accounted for 28, 38, and 11% of the total OA, respectively. Additionally, a combined organic and inorganic PMF analysis revealed two further factors: one enriched in nitrates and another rich in sulphates of organic and inorganic origin. The PTR_{CHARON} factorisation could identify four primary sources from residential heating: one from oil combustion and three from wood combustion, categorised as low temperature, softwood, and hardwood. Collectively, all residential heating factors accounted for 79% of the total OA. Cooking and road transport were also recognised as primary contributors to the overall emission profile provided by PTR_{CHARON}. All PMF analyses could apportion a single oxygenated secondary organic factor. These results demonstrate the complementarity of the two instruments and their ability to describe the complex chemical composition of PM_1 and the related sources. This work further demonstrates the capability of PTR_{CHARON} to provide both qualitative and quantitative information, offering a comprehensive understanding of the organic aerosol sources. Such insights into the sources of sub-micron aerosols can ultimately assist environmental regulators and citizen efforts to improve air quality in Fairbanks and the rapidly urbanising regional sub-Arctic areas.

Keywords PM_1, mass spectrometry, source apportionment, organic and inorganic aerosol, Fairbanks, Arctic cities, air quality, CHARON PTR-ToF MS, HR-ToF AMS, residential heating, wood combustion

1 Introduction

Extremely cold urban regions of the Earth, such as in the Arctic, experience poor dispersion of atmospheric pollution, especially during the wintertime, when the unique meteorological characteristics, such as extremely low solar radiation and strong radiative cooling at the surface, are coupled with enhanced local anthropogenic emissions from heating, industry, and transport. A good example is the sub-arctic city of Fairbanks, Alaska, where air quality standards are frequently violated during the winters with concentrations of fine particulate matter (i.e., with aerodynamic diameters smaller than 2.5 µm; $PM_{2.5}$) exceeding the 24-h limit of 35 µg/m^3 defined by EPA's National Ambient Air Quality Standards (Dunleavy and Brune, 2020; Epa, n.d.). Not only is Fairbanks one of the cities with the most polluted wintertime air in the US, but it has also been declared a 'moderate non-attainment area' since 2009, and due to the persistence of the problem, it was reclassified as a 'severe non-attainment area' in 2017. Increased local anthropogenic emissions and poor atmospheric dispersion due

to strong surface-based temperature inversions (> 0.5°C/m in the lowest 10 m above the ground) are major causes of wintertime pollution in the region (Tran and Mölders, 2011; Mayfield and Fochesatto, 2013). Many research studies have recognised biomass combustion as the major source of aerosol in Fairbanks (Ward et al., 2012; Wang and Hopke, 2014; Kotchenruther, 2016; Ye and Wang, 2020; Haque et al., 2021) that drives overall $PM_{2.5}$ concentrations across the city during strong temperature inversion conditions (Robinson et al., 2023). A comprehensive study covering three winters from 2008–2011 apportioned 60–80% of $PM_{2.5}$ mass at four locations in Fairbanks to emissions from residential wood stoves, open burning of biomass, outdoor boilers, and other solid-fuel combustion. (Ward et al., 2012). Source apportionment of year-round $PM_{2.5}$ in the past two decades [2008–2009 (Haque et al., 2021), 2005–2012 (Wang and Hopke, 2014), 2009–2014 (Kotchenruther, 2016), and 2013–2019 (Ye and Wang, 2020)] also revealed woodsmoke as a major contributor to $PM_{2.5}$ loads [47.5% (Haque et al., 2021), 40.5% (Wang and Hopke, 2014), ~52% (Kotchenruther, 2016), and ~19% (Ye and Wang, 2020)]. Wildfire activity and residential wood combustion are the major sources in summer and winter, respectively. The persistent role of wood-burning emissions in shaping the air quality of Fairbanks during winters triggered the implementation of a two-stage burn restriction in 2015 by the Alaska Department of Environmental Conservation (ADEC). The ADEC advisories restricted the operation of solid-fuel heating devices and required alternative heat sources to be used on days with weak atmospheric dispersion and $PM_{2.5}$ levels exceeding 25 $\mu g/m^3$, as observed or forecasted (Fye et al., 2009; Czarnecki, 2017; Jentgen, 2022). Sulphate has been observed to be the second largest component of $PM_{2.5}$ mass in Fairbanks (Ward et al., 2012; Wang and Hopke, 2014), forming ~33% of the annual average $PM_{2.5}$ mass (Ye and Wang, 2020). Isotope analyses have revealed 62% of this $PM_{2.5}$ sulphate to be primary (e.g., from residential heating oil combustion) during the winters (Moon et al., 2023).
The aforementioned studies on air quality in Fairbanks have focused on $PM_{2.5}$ even though PM_1 has been recognised as the major cause of adverse health effects (Wang et al., 2015; Mainka and Zajusz-Zubek, 2019) due to its capability to spread deeper into the respiratory or cardiovascular systems (Meng et al., 2013; Liu et al., 2013; Chen et al., 2017). Currently, efforts to monitor PM_1 are surprisingly scarce, even in 'non-attaining' cities, such as Fairbanks, underscoring the need for a better characterisation of sub-micron aerosols to understand local sources, chemical composition and ultimately to inform public health and support policy decisions.

Mass spectrometric techniques have advanced over the years, featuring greater mass accuracy, resolving power, and sensitivity. For instance, the Aerodyne high-resolution time-of-flight aerosol mass spectrometer (HR-ToF AMS; called AMS from hereon) is a well-established method for quantifying non-refractory NR-PM_1. Aerosol vapourisation at high temperatures and electron ionisation result in substantive molecular decomposition, facilitating quantification with high time resolution (Decarlo et al., 2006), but at the cost of molecular-level information. This limitation has encouraged the rise of

complementary techniques. For instance, extractive electrospray ionisation (EESI)-ToF MS has been successfully deployed in Beijing (Tong et al., 2021) and in Zurich to resolve multiple OA sources (Stefenelli et al., 2019a; Qi et al., 2019). Although the instrument provides molecular-level information, its quantitative response is variable and selective for polar species, preventing its independent application for ambient measurements. Other measurement methods, such as thermal desorption aerosol GC/MS flame ionisation detector (TAG)(Williams et al., 2006) and filter inlet for gases and aerosols chemical ionisation (FIGAERO-CIMS)-ToF MS (Lopez-Hilfiker et al., 2014), similarly offer better chemical resolution than the AMS, but a lower temporal resolution. Semi-continuous measurements, such as those from TAG and FIGAERO-CIMS, may not capture the rapid variation in sources.

To improve the analysis of sub-micron OA in ambient air, a novel inlet system called the chemical analysis for aerosol online (CHARON) was developed to collect real-time measurements (Eichler et al., 2015). This inlet minimises thermal and ionisation-induced fragmentation of sampled OA by employing a low-temperature vapourisation system (150°C ≤) and coupling with a relatively softer ionisation method, such as the proton-transfer reaction (PTR). The CHARON PTR-ToF MS (called PTR_{CHARON} from hereon) was successfully used for the characterisation of OA from ship exhaust (Eichler et al., 2017), ambient OA in Lyon, France, and Valencia, Spain, and OA source apportionment in Innsbruck, Austria (Müller et al., 2017). Recently, the inlet was used to quantify individual compounds in laboratory-generated secondary organic aerosol (Lannuque et al., 2023) and complex mixtures, such as vehicular gasoline emissions and atmospheric organic matter (Piel et al., 2019; Kostenidou et al., 2024). The system can also measure gas-phase species, creating the opportunity to explore VOC precursor emissions or phase partitioning (Peng et al., 2023; Gkatzelis et al., 2018). Overall, PTR_{CHARON} and AMS are complementary techniques; the former features molecular level information of the OA faction but has limited ability to detect particles below 150 nm (Eichler et al., 2015); the latter covers smaller particle size range (i.e., > 60 nm) and detects inorganic components too (Decarlo et al., 2006). Together, they provide an excellent combination of real-time and quantitative data on atmospheric ambient aerosol.

The detailed composition of sub-micron aerosol in Fairbanks and other anthropogenically influenced sub-Arctic regions – is still not well understood. To address this issue, we deployed a PTR_{CHARON} and an AMS in the urban centre of Fairbanks during the ALPACA (Alaskan Layered Pollution and Chemical Analysis) campaign as part of the French CASPA (Climate-Relevant Aerosol Sources and Processes in the Arctic) project in January–February 2022 (Simpson et al. 2024). We aimed to determine the composition, concentrations, and sources of atmospheric NR-PM_1. In this paper, we present (i) an intercomparison of the performance of the two instruments focusing on OA quantitation, (ii) the identification of major OA sources in Fairbanks, and (iii) the source apportionment of organic and inorganic aerosol (e.g., ammonium, nitrate, and sulphate). These findings highlight the synergistic

benefits of combining multiple analytical techniques and emphasise how soft ionisation mass spectroscopic methods enhance molecular-level insights into particulate organic carbon. This integrated approach advances our understanding of the complex composition of particulate matter, offering valuable contributions to environmental characterisation and source apportionment studies.

2 Methodology

2.1 Field campaign

The data presented in this study were collected during the ALPACA campaign in Fairbanks, Alaska, US, from January 20 to February 26, 2022. ALPACA is an international collaborative field experiment to understand sources of outdoor and indoor air pollution in the cold and dark conditions of Fairbanks' winter. The scientific objectives and broad preliminary findings of the experiment were recently reviewed (Simpson et al. 2024). All instruments used for this study were housed in a trailer parked at the Community and Technical College (CTC) of the University of Alaska, Fairbanks (64.84064°N, 147.72677°W; 136 m above sea level). The CTC is in the urban core of Fairbanks, close (within 40 m) to a central downtown road and parking area (Simpson et al. 2024); residential activities dominate the west of this locality, while the north and east have commercial activity.

The trailer was equipped with a suite of particle counters and mass spectrometers, featuring high temporal resolutions (ranging from 10 seconds to 2 minutes). A scanning mobility particle sizer (SMPS) and a multi-angle absorption photometer (MAAP) were utilised to measure the distribution of particles sized 15.1 to 661.2 nm and black carbon concentrations, respectively. A separate inlet was used for PM_1/$PM_{2.5}$/PM_{10} measurements conducted with a commercial optical particle counter (model OPC 1.109, Grimm Aerosol Technik) at a time resolution of 1 min. Two mass spectrometers, PTR_{CHARON} (150–1000 nm) and AMS (60–700 nm) were connected to the same inlet that sampled air at 3.5 meters above ground level through a short (≈ 1 m) stainless tube with a 1/2" outer diameter extending through the trailer roof. A HEPA filter was placed upstream of the inlet for an hour at regular intervals (twice a week) to measure the instrumental background. Additionally, meteorological data, including ambient temperatures at 3 and 23 m; wind speed and direction; and trace gases, namely CO, SO_2, O_3, NO and NO_2, were recorded as described in a previous study associated with the campaign (Cesler-Maloney et al., 2022).

2.2 Instrumentation

2.2.1 PTR-ToF MS: operation and data processing

The OA was quantified with a PTR-ToF MS (PTR-TOF 6000 X2, Ionicon Analytik GmbH, Austria) coupled to a CHARON inlet in near real-time at 20-s temporal resolution, i.e., the PTR_{CHARON}. The CHARON inlet has been described in detail by Eichler et al. (Eichler et al., 2015), and its applications were further evaluated and improved in subsequent studies (Müller et al., 2017; Leglise et al., 2019; Müller et al., 2019; Piel et al., 2019; Peng et al., 2023). Here, the PTR-ToF MS was configured to alternate between sampling of ambient air to measure VOCs for 15 minutes (not included in the current study) and sampling of particulate matter through the CHARON inlet for 45 minutes. The instrument was operated at a low E/N of 65 Td (i.e., drift voltage/pressure; pressure, temperature, and voltage of the drift tube were set at 2.6 mbar, 120°C, and 265 V) and in RF mode for optimal sensitivity. The thermodesorber was operated at 150°C and 8 mbar; this combination of moderate temperature with low pressure expands the range of detection to include ELVOCs as well (Piel et al. 2021). Raw data was obtained as described in **Section S1** and pre-processed with the Ionicon Data Analyzer (IDA, version 1.0.0.2), followed by post-processing (i.e., background subtraction, conversion of raw signal to mixing ratios, temporal averaging, PMF input generation) with an in-house data processing tool, PeTeR Toolkit (version 6.0; Igor 6.37). The error matrix was also calculated by PeTeR, taking into account uncertainties in ion counts and background signals. Among the resolved 1118 ions spanning the range of *m/z* 50–425, only 336 were retained above the S/N, and 318 ions could be given a molecular formula based on the criteria described in **Section S2**. PTR ToF MS records raw signals in counts per second (cps) that were converted to mixing ratios according to the molecular identity determined for the detected ions and their protonation efficiencies (further details in **Section S1**). For comparison with the AMS, mixing ratios were converted to mass concentrations, i.e., $\mu g/m^3$, using **Equation S2**. Mass concentrations calculated for the PTR_{CHARON} require a critical correction for the enrichment of sampled OA in the aerodynamic lens of the CHARON inlet (Eichler et al., 2015; Müller et al., 2017); further details are provided in **Section S3**. Total (or bulk) OA at a given point in time was the sum of mass concentrations of all ions, which was corrected for fragmentation using a previously reported method (Leglise et al., 2019), which increased the total OA mass concentrations by 17%.

Species with $m/z > 50$ were retained for PMF of OA, as molecules between *m/z* 18–50 were presented in low concentrations and are expected to be too volatile to be present in OA and were likely detected by PTR_{CHARON} as artefacts from the denuder. Time series were averaged to 2 minutes (from 20 seconds), and two matrices (*m/z* × time points) were extracted: (i) ion concentrations and (ii) their measurement

uncertainties, using PeTeR. The final matrices had the following dimensions: 336 × 17,986. Where required, ion intensities (in either ppb or µg/m^3) were normalised to the sum of all measured intensities.

2.2.2 HR-ToF AMS: operation and data processing

$NR\text{-}PM_1$ was monitored with 1-minute time resolution by a high-resolution time-of-flight mass spectrometer (AMS) (Aerodyne Research Inc., Billerica, USA), extensively described by Decarlo et al., (2006) and Canagaratna et al.(2007). Briefly, ambient particles are sampled through a critical orifice, focused into a narrow beam by an aerodynamic lens, accelerated toward a standard vapouriser heated at 600°C, and then ionised by electron impact (70 eV at 10^{-7} torr). Finally, the ions are analysed by a time-of-flight mass spectrometer. Standard calibrations were performed using 300 nm size-selected dried ammonium nitrate and ammonium sulphate particles at the beginning and the end of the campaign. Nitrate-equivalent values of sample mass concentrations were converted by applying relative ionisation efficiencies (RIEs) for organics, nitrates, ammonium, sulphate, and chloride (1.4, 1.1, 3.15, 1.93, and 1.3, respectively). Collection efficiency (CE) has been calculated in PIKA using the composition-dependent CE (CDCE) method, following the approach of Middlebrook et al. (2012). The calculated CE values ranged from 1.00 to 0.35.

Data was averaged to 2 minutes and extracted as concentration and measurement uncertainty matrices (*m/z* × time points) using SQUIRREL version 1.65 and PIKA version 1.25 in Igor 8.04. Separate matrices (and subsequently PMF) were prepared for organic only (abbreviated AMS_{org}) and by combining organic and inorganic species (abbreviated $AMS_{org+inorg}$). The inorganic species included in the analyses were nitrate (*m/z* 30, NO^+ and 46, NO_2^+), sulphate (*m/z* 48, SO^+; 64, SO_2^+; 80, SO_3^+; 81, HSO_3^+; and 98, $H_2SO_4^+$), ammonium (*m/z* 15, NH^+; 16, NH_2^+; and 17, NH_3^+), and chloride (*m/z* 35, Cl^+ and 36, HCl^+). Error matrices were calculated by PIKA based on uncertainty in ion counts, background signal, air beam correction, and electronic noise (Sueper, 2014). Atomic O/C and H/C ratios were calculated based on established methods (Aiken et al., 2007; Aiken et al., 2008; Canagaratna et al., 2015). Where needed for comparison with the PTR_{CHARON}, mass concentrations of PAHs were estimated from fragments as described previously (Herring et al., 2015), and levoglucosan was estimated as detailed in **Section S4**.

Species with *m/z* 12–120 were retained for PMF in this study, excluding important PAHs detected up to *m/z* 252; such PAHs were used as external tracers for factor identification. All PAHs were included in total OA quantification and associated comparisons. This exclusion is expected to cause underestimation below 2% of the mass of some factors, particularly HOA (hydrocarbon-like organic

aerosol) and BBOA (biomass-burning organic aerosol). Final matrices from AMS_{org} and $AMS_{org+inorg}$ analyses had the following dimensions: 193 × 24,762 and 205 × 24,762, respectively.

2.3 Source apportionment: Positive matrix factorisation

Source apportionment was performed using a PMF implemented in the multilinear engine (ME-2) (Paatero, 1997a, 1999). The PMF was configured and analysed using the SoFi (Source Finder) Pro interface (Canonaco et al., 2013) (version 8.4.1.9.1; Igor 8.04). PMF is a descriptive mathematical algorithm that describes the input data, i.e. measurements of several variables collected over time (here, *m/z* × sampling time points), as a linear combination of factors that have constant mass spectra associated with temporally varying concentrations of the spectral constituents (Paatero, 1997b; Paatero and Tapper, 1994). The mathematical expressions and functions of the PMF algorithm have been exhaustively detailed in previous studies (e.g., refs. (Tong et al., 2021; Stefenelli et al., 2019a; Chen et al., 2022; Chazeau et al., 2022), etc.). Below, we summarise the user-defined configurations applied in SoFi Pro to optimise the PMF of our datasets, PTR_{CHARON}, AMS_{org}, and $AMS_{org+inorg}$.

2.3.1. General methodology for PMF analysis

Preliminary PMF was performed without using *a priori* information to explore factor variability and source contributions to guide the selection of an optimal solution before applying constraints. We considered solutions ranging from 3 to 13 factors, applying a step-wise, cell-wise down-weighting approach: variables with S/N < 0.2 ("bad" variables) were down-weighted by a factor of 10, while those with 0.2 < S/N < 2 ("weak" variables) were down-weighted by a factor of 2 (Paatero and Hopke, 2003; Ulbrich et al., 2009). Upon establishing some primary factors, such as cooking and biomass burning, which were successfully identified in unconstrained trials, we narrowed the range of possible solutions by applying the a-value approach, which allows for improved factorisation by constraining the PMF with external data when available (Canonaco et al., 2013; Paatero, 1999). For instance, a factor profile from a PMF trial in the same experiment, a time series from an external tracer, or a well-established factor profile for a source from another experiment may be provided to the PMF as an 'anchor/vector' around which it can build a factor in its overall solution. The extent to which each PMF factor can diverge from the anchor is defined by the value of *a* (Tong et al., 2021), which varies from 0 to 1. This anchor can be provided for one or multiple factors and has been proven to improve the quality of PMF solutions compared to unconstrained trials (Tong et al., 2021; Stefenelli et al., 2019a; Chen et al., 2022).

Currently, there are no objective criteria for choosing the optimal number of factors; however, several criteria have been proposed in the literature to inform an appropriate choice (Chen et al., 2022; Zhang et al., 2011; Ulbrich et al., 2009; Crippa et al., 2014). The PMF solutions reported here were primarily

selected based on their physical meaning, which was determined by the presence of known tracer compounds in the factors and temporal correlation with co-located measurements of external tracers (e.g., NO_x, SO_2). We selected eight-, four-, and six-factor solutions from PTR_{CHARON}, AMS_{org}, and $AMS_{org+inorg}$, respectively. The justification for these solutions is presented in **Table S2**. Once the most suitable solution, i.e., the base-case, was established, bootstrap analyses were performed to assess its stability, evaluate uncertainties, and conduct a sensitivity analysis on the range of *a*-values used. In an unblocked bootstrapping approach, the original matrices (both data and error) are perturbed by random resampling of the rows to create a new input of the same dimensions, resulting in some duplications and deletions throughout the input (Paatero et al., 2014). The need and application of this approach differed between the PTR_{CHARON} and the two AMS datasets, as discussed in **Sections S5** and **S6**, respectively. Ancillary data on particle size distribution have been associated with mass spectrometry data in an additional PMF analysis (**Section S7**). Finally, the quality of the solutions was assessed by the Q/Q_{exp} values and from key diagnostic plots of residuals, as well as the statistical stability across multiple runs (**Figure S5–S7**).

3 Results and Discussion

3.1 Campaign overview

Figure 1 summarises the meteorological conditions, chemical composition and particle size distribution of NR-PM_1 observed from January 20 to February 26, 2022. High aerosol loads coincided with poor atmospheric dispersion due to low wind speeds (<2 m/s) and low temperatures (below -10°C), associated with strong surface temperature inversions. The temperature differences between 23 and 3 m above sea level ranged from 3°C to 10°C. The average values of BC and NR-PM_1 measured with the MAAP and AMS were **1.4 ± 1.4 µg/m^3** and **8.3 ± 9.3 µg/m^3**, respectively. During intense pollution events, the daily average concentrations of NR-PM_1 were **24–27 µg/m^3**. During the same sampling period at the NCore site (Fairbanks), $PM_{2.5}$ values of ~25 and ~29 µg/m^3 were reported (Robinson et al., 2023). Ancillary OPC measurements at the CTC site showed that the hourly PM_1 mass comprised up to 99% of the $PM_{2.5}$. Organics were the predominant component of NR-PM_1 throughout the campaign, constituting **~66 ± 11**% of its total mass, while chloride, ammonium, nitrate, and sulphate-contributed **2 ± 3, 3 ± 3**, **6 ± 4**, and **22 ± 10**%. This finding aligns with previous studies in Fairbanks, where OA was the largest component of $PM_{2.5}$ mass (Ward et al., 2012; Ye and Wang, 2020; Robinson et al., 2024). Specifically, according to a recent study from 2020 to 2021, ACSM analysis during wintertime demonstrated that inorganics formed less than 25% of the $PM_{2.5}$ mass, with sulphate (~10%) and nitrate (~8%) being the predominant components (Robinson et al., 2024). Despite the different average concentrations, the fractional contributions of these non-refractory components remained

almost invariable throughout the campaign (**Figure 1D**). Detailed molecular-level composition of organics with the PTR_{CHARON} reveals a large majority of organics to comprise only C, H, and/or O atoms, while only **~9 ± 4%** of the OA_{CHARON} mass measured with this instrument was attributable to heteroatomic molecules, including organonitrates and organosulphates (**Figure 4 and S8**). Generally, heteroatomic species cannot be distinguished at a resolving power of 5000 FWHM in complex environmental mixtures, such as atmospheric aerosol (Reemtsma, 2009). In this study, based on the low formula error and lack of an appropriate alternate, we gave 53 low-concentration ions (< 2% of the total signal) CHOS or CHNO identities. However, due to the low confidence in their formula assignments, they were not considered for factor identification. Prominent peaks include *m/z* 217.09 ($C_{12}H_{12}N_2O_2$), 219.09 ($C_{15}H_{10}N_2$), 123.05 ($C_4H_{10}O_2S$), and 151.08 ($C_6H_{14}O_2S$).

On average, the OA mass loading recovered by PTR_{CHARON} (i.e., OA_{CHARON}) accounted for approximately 85% of the OA mass measured by the AMS (i.e., OA_{AMS}). While the two instruments showed a good temporal agreement (R^2 = 0.60), as depicted in **Figures 2A–B**, measurements were biased either toward the AMS_{org} or the PTR_{CHARON} (i.e., distributed away from the 1:1 line in the scatter plot of **Figure 2C**) during different periods of the campaign. These trends could be explained by the variation in relative contributions of two major emission sources identified by both instruments in this study: on-road transport and biomass burning. OA_{CHARON} was comparable to OA_{AMS}, when the relative contribution of $BBOA_{AMS,org}$ was more than 50% of total OA_{AMS} and $HOA_{AMS,org}$ (i.e., $transport_{CHARON}$) was less than 10% (**Figure 2D–E**). Similar trends were observed for some major constituents of BBOA, e.g., levoglucosan and a PAH ($C_{20}H_{12}$), as shown in **Figure S9**. Part of such discrepancy can be traced back to the size transmission of particles, where sub-100 nm urban vehicular emissions are underestimated by the PTR_{CHARON} (Guo et al., 2020; Pikridas et al., 2015; Louis et al., 2017; Kostenidou et al., 2020), and larger than 100 nm biomass burning emissions (Reid et al., 2005) are estimated well (Janhäll et al., 2010). Another part of the quantitative difference can be explained by the PTR limitation in ionisation and the induced fragmentation of analyte ions. Tests conducted in our laboratory with five C_{16}–C_{26} alkanes as markers of vehicle emissions revealed that they undergo extensive fragmentation, resulting in 2–4 times underestimation of their actual concentrations. In line with this, the ineffective ionisation of saturated alkanes by PTR (Ellis and Mayhew, 2014) and their tendency to undergo dissociative ionisation (Gueneron et al., 2015) have also been reported.

3.2 Source apportionment

3.2.1. Overview of source apportionment

A four-factor solution was selected for the AMS_{org} measurements with three primary factors (i.e., HOA, COA, and BBOA) and an oxygenated or aged OA factor (i.e., OOA). The mass spectra and time series

are presented in the supplement (**Figure S10**). Counterparts of these four factors were diagnosed in $AMS_{org+inorg}$ based on a high temporal correlation ($R^2 > 0.9$; Table S4), along with two additional factors: a sulphur-rich factor (labelled sulph-OA) and a nitrate-rich factor (labelled AmNi) (**Figure 3**). An eight-factor solution was selected for PTR_{CHARON} and is summarised in **Figures 4 and 5**. To differentiate between corresponding factors retrieved from the different datasets, they have been assigned unique subscripts, e.g. $COA_{AMS,org}$, $COA_{AMS,org+inorg}$, or COA_{AMS} (i.e., referring to both AMS datasets), or COA_{CHARON}. Amongst the three datasets, COA, HOA (labelled 'transport' in PTR_{CHARON} analyses), and OOA were common. A single BBOA factor was observed in AMS_{org} and $AMS_{org+inorg}$, while four chemically distinct but closely co-varying counterparts were detected by PTR_{CHARON}. 3.2.2. Organic aerosol from residential heating.

Both AMS analyses indicate that biomass burning is a major source of PM_1 during the ALPACA campaign. On average, BBOA contributed **1.5 ± 1.9 µg/m³** (**28 ± 18%** of total OA_{AMS}) and **1.6 ± 2.2 µg/m³** NR-PM_1 (**19 ± 14%** of total NR-PM_1 mass). The mass spectra of $BBOA_{AMS}$ featured a strong peak at *m/z* 60 ($C_2H_4O_2^+$) and 73 ($C_3H_5O_2^+$) (**Figure S10A–B**). These fragments are markers of anhydrosugars in wood-forming polymers, such as cellulose. Wood combustion has previously been estimated to be the largest emitter of aerosols in Fairbanks and surrounding areas, where it may produce as much as 80% of the aerosol load. Wood burning emissions are also the major driver of the spatial variability of $PM_{2.5}$ and BC in Fairbanks during strong atmospheric temperature inversions. Other typical residential heating sources of emissions in Fairbanks include coal, gas, and fuel oil.

The $BBOA_{AMS}$ factor was strongly correlated with PAHs ($R^2 \geq 0.7$), while a moderate correlation was observed with SO_2 ($R^2 = 0.4$) (**Table 1**). While PAHs are a major component of biomass combustion emissions, the emission of SO_2 is largely associated with coal and oil combustion (Smith et al., 2011; Dunleavy and Brune, 2019). However, the AMS was unable to distinguish between multiple combustion-related sources. As shown in the diurnal plots in **Figure 3**, the concentration of the $BBOA_{AMS}$ factor enhanced at ~1800 AKST, stayed stable through the night and then decreased in the early morning. Its lowest mass concentrations occurred during the afternoon (1300–1500 AKST). Therefore, $BBOA_{AMS}$ was associated with residential heating, i.e., the combustion of various fuels by residents within their homes (non-commercially), such as in wood-burning stoves, furnaces, and boilers, for heating their living spaces. We did not find evidence of OA or NR-PM_1 from commercial heat sources, such as power plants, likely due to their small contribution to surface-level aerosol, as smokestacks typically lie above the inversion layer.

PTR_{CHARON} apportioned **2.6 ± 3.4** µg/m³ of OA_{CHARON}, on average, to four distinct residential heating-related sources expressed as ResH1–4 (**62 ± 26%** of total OA_{CHARON}). These factors closely co-varied

in time and were correlated reasonably well (R^2 = 0.5–0.7; **Table S5**) with the $BBOA_{AMS}$ factor. In addition, combining all four residential heating-related factors in PTR_{CHARON} into a composite factor increased the correlation (R^2) with AMS_{org} and $AMS_{org+inorg}$ to 0.79 and 0.82, respectively, suggesting that PMF was unable to effectively separate these closely co-varying residential heating factors in the AMS dataset.

The four factors from PTR_{CHARON} were identified as different sources based on the distribution of key marker species and their correlation with external (e.g., trace gases, etc.) and internal (e.g., PAH) influences. Levoglucosan is used here as an internal tracer of biomass burning, being relatively stable under atmospheric conditions (Fraser and Lakshmanan, 2000). Protonated levoglucosan (*m/z* 163) and its fragments (at *m/z* 85, 127, and 145) were found in ResH1, ResH4, and ResH2 with **30, 26, 14%** of the total signal, respectively **(Figure S11**), suggesting that they originate from biomass wood-burning (**Figure 4 and S11**). These three factors collectively accounted for **2.1 ± 2.5 µg/m^3** (**47 ± 20%)** of total factorised OA_{CHARON}.

ResH1 includes low-temperature combustion markers*:* This factor is small as it contributes to only an average of **0.5 ± 0.5 µg/m^3** (**14%**) of the total OA_{CHARON}, but it contains the highest fraction of levoglucosan (~30%). Approximately 65% of the total signal of ResH1 is due to compounds with six or fewer carbon atoms, compared to heavier species present in the other factors (**Figure S13**). The most abundant species are at *m/z* 69.03 (C_4H_4O; furan) (Palm et al., 2020; Jiang et al., 2019), m/z 87.04 ($C_4H_6O_2$; oxobutanal) (Brégonzio-Rozier et al., 2015), *m/z* 97.03 ($C_5H_4O_2$; furfural), *m/z* 109.0286 ($C_6H_4O_2$; benzoquinone) (Stefenelli et al., 2019b) and *m/z* 115.04 ($C_5H_6O_3$; methyl-dihydrofuran) (Koss et al., 2018). Consistent with these molecular formulae, the concentration-weighted average O/C of ResH1 was relatively higher (i.e., 0.42) compared to other residential heating factors (O/C = 0.2–0.3). The most abundant species observed in ResH1 can be attributed to depolymerisation reactions occurring during low temperatures and the early stages of the combustion process (Collard and Blin, 2014; Sekimoto et al., 2018).

ResH2 and ResH4 include OA from hardwood and pinewood combustion, respectively: Two more factors associated with wood-burning were ResH2 and ResH4. Their average concentrations were **1.1 ± 1.9** and **0.8 ± 0.9 µg/m^3**, respectively, corresponding to **28** and **20%** of the OA_{CHARON} (**Figure 6**). The ResH2 was the dominant factor in the PMF and could reach **~37 µg/m^3** during the most severe pollution episodes. Both factors were associated with particles greater than 300 nm (**Figure S12**), typical of woodsmoke (Glasius et al., 2006), and presented unique molecular signatures of different wood types (**Figure S11)**. Generally, the specific nature of wood cannot be inferred unambiguously because the emissions of known marker species, such as levoglucosan or methoxy phenols, vary not just with fuel

used and its quality but also with the type of heating appliance, operational conditions, appliance efficiency, and stage in the combustion cycle (Fine et al., 2002; Alves et al., 2017). Regardless, several studies (Fine et al., 2002; Schauer and Cass, 2000; Kawamoto, 2017) have distinguished between softwood and hardwood by investigating the presence of marker compounds, which were also observed in our study, such as substituted phenols and resin acids **(Figure S11).**

ResH2 featured an abundance of methoxy phenols, including $C_7H_8O_2$ (guaiacol), $C_8H_{10}O_3$ (syringol), $C_{10}H_{10}O_3$ (coniferaldehyde), $C_6H_6O_2$ (benzenediol or methylfurfural), and $C_8H_{10}O_2$ (creosol), that collectively accounted for ~9% of the total signal, compared to 1, 2, and 2% in ResH1, ResH3, and ResH4, respectively. These compounds are important products of lignin pyrolysis in birch, aspen, and spruce and are usually detected in the gas phase at mild ambient temperatures (Kong et al., 2021). Guaiacol and syringol are depolymerisation products of guaiacyl and syringyl units of lignin at 200–400°C, and they rapidly transition to catechols, cresols, and phenols during secondary pyrolysis reactions at 400–450°C (Kawamoto, 2017). While guaiacols are emitted by both hardwood and softwood, semi- or low-volatility substituted syringols are emitted in higher amounts by hardwood combustion (Kawamoto, 2017; Fine et al., 2002, 2001; Schauer and Cass, 2000). In this study, derivatives of guaiacols, including $C_{10}H_{12}O_2$ (eugenol), $C_{10}H_{14}O_2$ (4-propyl guaiacol), and $C_{10}H_{10}O_3$ (coniferaldehyde) presented higher "relative concentration" (**Equation S3**) of 0.56–1.41 for ResH2 and ResH4 compared to ResH1 (<0). Other compounds, such as $C_8H_8O_3$ (vanillin), $C_9H_{10}O_3$ (acetovanillone), $C_{10}H_{12}O_3$ (propiovanillone), and $C_{10}H_{12}O_4$ (methyl homovanillate), were predominantly found in ResH2. Similarly, substituted syringols, i.e., $C_{11}H_{14}O_3$ (methoxy eugenol), $C_{10}H_{12}O_4$ (acetosyringone), and $C_{11}H_{14}O_4$ (syringyl acetone, propionyl syringol, or sinapyl alcohol) were almost entirely associated with ResH2 as well. These compounds have been reported as markers of hardwood burning (Fine et al., 2001), implying a greater contribution of hardwood emissions to the ResH2 factor. In Alaska, relevant hardwood species include deciduous leafy trees, i.e., paper birch, balsam poplar, quaking aspen, etc. (ADEC, 2023).

The ResH4 factor presented a unique fingerprint characterised by oxygenated molecules bearing more than 13 carbon atoms (**Figure S13**), such as $C_{16}H_{30}O_6$ (*m/z* 319.21), $C_{20}H_{28}O_2$ (*m/z* 301.21), $C_{20}H_{18}O_4$ (*m/z* 323.12), $C_{20}H_{30}O_2$ (*m/z* 303.24) and $C_{22}H_{18}O$ (*m/z* 299.14), in addition to the levoglucosan marker ions (26% of the total signal). The intense signals from *m/z* 301 ($C_{20}H_{28}O_2$) and *m/z* 303 ($C_{20}H_{30}O_2$) (**Figure S11**) are likely related to resin acids, dehydroabietic acid and abietic acid, respectively, which are almost exclusively emitted from the thermal alteration of resins in coniferous species, and thus, are indicative of softwood burning (Simoneit, 2002, 1999). Due to the presence of these compounds, ResH4 was interpreted as an OA factor influenced by softwood combustion. Softwood species in Alaska include trees with needles and cones, e.g. hemlock, cedar, and spruce (Adec, 2023).

ResH3 includes OA from heating oil combustion: This factor contributed to **16 ± 9%** of the total OA_{CHARON} (**0.6 ± 0.6 µg/m^3**). It showed the characteristic diurnal pattern of residential heating as it correlated quite well (R^2 = 0.56) with $BBOA_{AMS,org.}$ However, its chemical composition differed from that of the other residential heating factors. Notably, levoglucosan contributed to a smaller fraction of the total signal of ResH3 (i.e., 9%) compared to other residential heating factors (14–30%; **Figure S11**), while PAHs represented a much larger fraction of its total signal (for instance, 30, 31, and 29% of $C_{16}H_{10}$ (*m/z* 203.09), $C_{18}H_{12}$ (*m/z* 229.10), and $C_{20}H_{12}$ (*m/z* 253.10); **Figure S13**). These PAHs could be fluoranthene (or pyrene), naphthacene (or benzo[*x*]anthracene, chrysene), and benzo(*x*)pyrene (or benzo(*x*)fluoranthene)), which have been reported in emissions of light oil combustion (Bari et al., 2009). Additionally, ResH3 was strongly correlated with SO_2 (R_2 = 0.61), compared to a lower correlation ($R^2 \leq 0.47$) with the other residential heating factors. Residential combustion of heating oil is an important source of SO_2 in Fairbanks, compared to wood and coal, due to ~2/3rd of the households using oil-fired space heaters and the high sulphur content of > 1600 ppm in fuel oils commonly consumed here (e.g., #1 and #2 fuel oil and waste motor oil are relevant in Fairbanks)(Dunleavy and Brune, 2019). Consistent with the possibility of the ResH3 factor being associated with fuel oil emissions, the factor is characterised by particles smaller than 100 nm (**Figure S12**) and due to the CHARON inlet's cut-off, its mass concentration was possibly underestimated.

3.2.3. Hydrocarbon-like organic aerosol

The HOA_{AMS} factors were characterised by notable peaks at *m/z* 43 ($C_3H_7^+$), 57 ($C_4H_9^+$), 71 ($C_5H_{11}^+$), 85 ($C_6H_{13}^+$), and 99 ($C_7H_{15}^+$), belonging to $[C_nH_{2n+1}]^+$ series, typical of *n*- and branched alkanes. Additional peaks at *m/z* 55 ($C_4H_7^+$), 69 ($C_5H_9^+$), 81 ($C_6H_9^+$), 83 ($C_6H_{11}^+$), 95 ($C_7H_{11}^+$), 97 ($C_7H_{13}^+$), 107 ($C_8H_{11}^+$), 109 ($C_8H_{13}^+$), and 111 ($C_8H_{15}^+$) represented $[C_nH_{2n-1}]^+$ and $[C_nH_{2n-3}]^+$ series, related to cycloalkanes (McLafferty et al. 1993). These ions are associated with engine-lubricating oils, vehicular exhaust, and diesel fuel (Canagaratna et al., 2004). The HOA_{AMS} factors contributed **38 ± 20%** and **21 ± 14%** of the OA_{AMS} and NR-PM_1 mass, respectively (**Figures 6 and S14**).

The unconstrained PTR_{CHARON} analysis was unable to apportion a road transport-related factor; however, by constraining the factorisation with the time series of a mobile gasoline factor, identified in the gas-phase PTR-ToF MS analyses of the ALPACA campaign (Temime Roussel et al., 2022), a small road transport-associated factor was identified. For instance, this latter was strongly correlated with black carbon and NO_x (R^2 of 0.58 and 0.66; **Table 1**) and featured high contributions of C_8H_{10} (xylene; ethylbenzene), C_7H_8 (toluene), and C_6H_6 (benzene) (**Figures 4 and S11**). Despite exhibiting some reasonable diurnal trend peaking at the morning (0900 AKST) and evening (1700–1600 AKST) rush hours (**Figure 5**), the factor accounted for negligible concentrations (< 1 µg/m^3) and presented some

unlikely species, such as *m/z* 315.22 ($C_{21}H_{30}O_2$; possibly cannabidiol) absent in the unconstrained PMF. For instance, on average, **2.1 ± 3.0 µg/m^3** of OA was associated with $HOA_{AMS,org}$, compared to only **0.1 ± 0.1 µg/m^3** for the road transport$_{CHARON}$ factor (**Figure 6**). These discrepancies are largely instrumental, partly due to the poor transmission of the small particles (<100 nm) by the CHARON inlet and the limited sensitivity towards hydrocarbons by PTR, but other possible biases can be due to heating oil OA signal interfering with the HOA_{AMS}, as discussed in **S8**.

3.2.4. Cooking organic aerosol

Another primary factor identified in Fairbanks was cooking, likely arising from residential or commercial activities around the CTC. The COA_{AMS} factor featured a high abundance of $C_xH_y^+$ ions, along with prominent O_1 fragments at *m/z* 55 ($C_3H_3O^+$), 84 ($C_5H_8O^+$), and 98 ($C_6H_{10}O^+$) originating from organic acids (Mohr et al., 2009) and used as diagnostic markers of COA in urban settings (Sun et al., 2011). The *f*55/*f*57 value (i.e., the ratio of fractions of $C_4H_7^+$ to $C_4H_9^+$) was ~3.00 for COA_{AMS}, compared to ~1.04 for HOA_{AMS} (**Figure S10D**). As a reliable tracer for COA remains unidentified in the AMS spectrum, a *f*55/*f*57 ratio >1 is considered a characteristic feature (Katz et al., 2021; Sun et al., 2011). The PMF analysis of PTR_{CHARON} also revealed a distinct COA factor dominated by long-chain fatty acids, $C_{18}H_{32}O_2$, $C_{18}H_{34}O_2$, and $C_{18}H_{36}O_2$, identified as linoleic, oleic, and stearic acids contributing to11, 16, and 4% to the total COA_{CHARON} mass (**Figure 4 and S11**). These fatty acids are commonly found in OA from cooking oil and meat (Katz et al., 2021; Mohr et al., 2009). The COA_{CHARON} contributed to a maximum of ~9% of the total OA_{CHARON} mass and exhibited a unique diurnal pattern visualised in **Figure 5** with a minor maximum in the afternoon (lunchtime) and a second maximum in the evening (dinnertime). The average absolute concentrations of COA were **0.6 ± 0.8** for the AMS and **0.1 ± 0.2 µg/m^3** for the PTR_{CHARON}. Such a discrepancy can be explained by the same reason discussed above and detailed in Section **S9**.

3.2.5. Oxygenated organic aerosol

Past source apportionment studies have reported multiple OOA factors differing in volatilities or oxygenation levels (e.g., Stefenelli et al., 2019a; Kumar et al., 2022; Cash et al., 2020). Here, we diagnosed only a single OOA factor in either AMS or PTR_{CHARON} measurements. Specifically, the OOA_{AMS} factors were identified based on a prominent peak at *m/z* 43 ($C_2H_3O^+$) and *m/z* 29 (CHO^+; **Figure S10A**) and showed a strong correlation (R^2 0.74) with OOA_{CHARON}. The average absolute concentrations of OOA_{CHARON} and $OOA_{AMS,org}$ were **0.4 ± 0.6** and **1.0 ± 2.1 µg/m^3**, respectively. Notably, the most intense ions in the mass spectrum of OOA_{CHARON} have been tentatively assigned to *m/z* 73.03 ($C_3H_5O_2$, e.g., methylglyoxal), *m/z* 99.04 ($C_5H_6O_2$, e.g., oxo-pentanal), *m/z* 113.06 ($C_6H_8O_2$,

e.g.,methyl-oxo-pentanal), *m/z* 127.08 ($C_7H_{10}O_2$; e.g., heptadienoic acid), *m/z* 137.06 ($C_8H_8O_2$; e.g., methoxy-benzaldehyde), *m/z* 167.10 ($C_{10}H_{14}O_2$), *m/z* 171.07 ($C_8H_{10}O_4$) and *m/z* 185.10 ($C_{13}H_{12}O$; e.g., benzyl phenol). Among these compounds, some have previously been associated with the atmospheric oxidation or photolysis of BBOA (Montoya-Aguilera et al., 2017; Lignell et al., 2013; Smith et al., 2020), while others could be due to the oxidation of aromatic VOCs detected originating from road transport (Temime-Roussel et al., 2022). Few other species overlapped with the residential heating tracers, notably *m/z* 163.06 ($C_6H_{10}O_5$; e.g., levoglucosan), *m/z* 179.08 ($C_{10}H_{10}O_3$; e.g., coniferaldehyde), and *m/z* 301.21 ($C_{20}H_{28}O_2$; e.g., dehydroabietic acid). However, given the prominence of wood burning as a major primary emission, the OOA is likely linked to BBOA. A recent study in Fairbanks identified wintertime OOA as a mixture of BBOA and SOA formed from non-photochemical processing using an ACSM (Robinson et al., 2024). The examination of *f*44 versus *f*60 in the AMS_{org} dataset plot (**Figure S10C)** is consistent with aged OOA derived from biomass burning, as previously demonstrated by Xu et al. (2023). Another recent source apportionment study using the HR-ToF AMS at a site close to the CTC did not identify an OOA factor, while BBOA, HOA, and a mixed primary factor (HOA, COA, etc.) comprised 45, 25, and 31% of total OA, respectively (Yang et al., 2024). A limited OOA formation is plausible due to reduced solar light exposure in this period of the year (Cesler-Maloney et al., 2024). However, the absence of OOA is more likely a result of an unresolved organic fraction.

Sulphate and OOA. An intriguing insight about the OOA factor emerged from the $AMS_{org+inorg}$ measurements, indicating a significant content of sulphur-containing compounds (**Figure S15**). The AMS does not distinguish among the different sulphur-containing species, but following guidelines from previous works (Chen et al., 2019; Schueneman et al., 2021), we could explore the ratio of sulphur fragments to investigate the presence of different species such as hydroxymethane sulphonate (HMS; $CH_2(OH)SO^{-3}$), HSO_4^- (bisulphite), SO_4^{2-} (sulphate) and (H_2SO_4) sulphuric acid. An organosulphate content of ~ **0.8 ± 1.3 µg/m^3** (**~20 ± 16%**) was then derived using the ratios of SO^+ and SO_2^+ ions against SO_3^+, HSO_3^+, and $H_2SO_4^+$ ions as detailed by Song et al., (2019). This value is in good agreement with previous reports from the same field campaign (Campbell et al., 2022; Robinson et al., 2024). Additionally, to mimic the potential matrix effects of wood burning OA on sulphate fragmentation patterns, AMS spectra from a solution of $(NH_4)_2SO_4$ mixed with various amounts of levoglucosan (i.e., 0–80% in mass) were compared to ambient data and PMF factors as shown in **Figure S16A**. Among the sulphate-rich factors, the $OOA_{AMS,org+inorg}$ exhibited lower HSO_3^+ to $H_2SO_4^+$ intensities, suggesting a higher fraction of organosulphate compounds, as is also evidenced in **Figure S16D–E** by the strong correlation between derived organosulphur fraction and sulphate-ions in the $OOA_{AMS,org+inorg}$ factor (R^2 = 0.85, slope = 0.57).

Further information on chemical composition was gathered by comparing AMS results with IC measurements from $PM_{0.7}$ filters sampled as part of another ALPACA study (Dingilian et al., 2024). Despite the good correlations between the two datasets, as shown in **Figure 7A,** the AMS underestimated sulphate, ammonium, and nitrate by 30%, 26%, and 35%, respectively (see **Section 2.2.2**). Both the total estimated organosulphur fraction and the $OOA_{AMS,org+inorg}$ factor presented robust correlations ($R^2 > 0.90$) with the $S_{(IV)}$ and HMS ions from filter analysis and a somewhat weaker correlation ($R^2 > 0.61–0.68$) with the SO_4^{2-} ion (**Figures 7 and S16F–I**). The $OOA_{AMS,org+inorg}$ factor was also strongly correlated with ammonium (AMS data $R^2 = 0.86$, **Table 1**; filter IC $R^2 = 0.77$, **Figure 7B**), potentially promoting the formation of $S_{(IV)}$ species (Campbell et al., 2024). This author also reported that $S_{(IV)}$ species, including HMS, represented the major secondary organosulphur component of $PM_{2.5}$ in Fairbanks during wintertime, contributing 26–41% of total sulphate (Campbell et al., 2022). Overall, the molecular-level composition of OOA from PTR_{CHARON} and the inorganic chemical information from $AMS_{org+inorg}$, as well as diurnal patterns with enhanced concentrations in the afternoon (**Figure 3**), are indicative of chemical daytime processing, underscoring the need for further exploration of the atmospheric processing pathways involved.

3.2.6. Additional insights from combined analysis of organic and inorganic AMS data

Two additional factors, sulph-OA (i.e., sulphur-rich OA) and AmNi (i.e., ammonium nitrate), were observed from the PMF of $AMS_{org+inorg}$ (**Figure 3**). Approximately 40–60% of these factors' masses comprised sulphur and nitrogen species (**Figure S15**).

Sulphur-rich organic aerosol: Sulph-OA is composed of sulphate 60%, organics 30%, ammonium 6% and nitrate 4%. The chemical composition was further explored via the $fHSO_3/fH_2SO_4$ analysis detailed in **Section 3.2.4**, as shown in **Figure S16A**, where the factor is positioned between H_2SO_4 and $(NH_4)_2SO_4$. The measured $[NH_4]/[SO_4]$ ratio was 0.07, considerably lower than the theoretical mass ratio of 0.38 and 0.18 of $(NH_4)_2SO_4$ and NH_4HSO_4, respectively, indicating an acidic nature of Sulph-OA (Chen et al. 2019). The factor was well correlated with SO_2 ($R^2 = 0.6$) and moderately correlated with the ResH3 factor (R^2 of 0.33). The factor was also associated with ultrafine particles in the 50–80 nm range (**Figure S12D**). Regardless of the low correlation, we speculate that ResH3 and sulph-OA originated from the same source, i.e., residential heating oil combustion, and their temporal disagreement may result from instrumental biases of the CHARON inlet in quantifying particles smaller than 100 nm (**Figures S12B and D**). For instance, as shown in **Figures S12E–F**, the organic ResH3 supersedes sulph-OA concentrations when larger particles are abundant, and it has lower concentrations for smaller particles.

This factor contained **0.6 ± 0.5 µg/m^3** (**~58 ± 26%**) of total sulphate measured with the AMS, and it dominated during the low-pollution periods, which were more frequent and lasted longer than the high-pollution events (**Figure 1**). Other primary factors, $HOA_{AMS,org+inorg}$, $COA_{AMS,org+inorg}$, and $BBOA_{AMS,org+inorg}$, contained an additional 11 ± 9% of the sulphate (**0.2 ± 0.2 µg/m^3**), so collectively, primary factors made up **69 ± 24%** (**0.7 ± 0.6 µg/m^3**) of total sulphate. This value is in close agreement with a previous ALPACA study that reported ~62 ± 12% of total SO_4^{2-} mass to be of primary origin (Moon et al., 2023).

AmNi factor. The second inorganic factor was composed of 35% nitrate, 14% ammonium, and 43% organics, accounting for 71 ± 23% of the total nitrate measured by the AMS (R^2 = 0.98). The average concentration of this factor and the nitrate species in it were **1.1 ± 1.6** µg/m^3 and **0.4 ± 0.5** µg/m^3. The factor was more abundant when NOx concentrations were high (above 130 ppbv)(**Figure S17B**); its diurnal trend peaked around 1400 AKST (Figure 3), roughly 3-4 hours after the morning peak of HOA_{AMS} and was associated with relatively small particles of 110 nm (**Figure S12D**). A high contribution of aliphatic moieties characterised the organic fraction, and according to the difference in mass concentrations of $HOA_{AMS,org}$ and $HOA_{AMS,org+inorg}$ of 13% (**Figure S17A**), we speculate that some organic components of $HOA_{AMS,org}$ were transferred to the AmNi factor (**Figure 6**). All these elements suggest a probable contribution from the vehicular emissions to this factor. The presence of inorganic compounds provided additional variables to the PMF, thereby improving the resolution of factors into distinct AmNi and $HOA_{AMS,org+inorg}$ factors.

4. Local environmental implications

During the period of the campaign, 12–48-hour-long ADEC advisories for wood-burning restrictions were implemented seven times. Variation in the relative contributions of ResH1–4 during these advisories is depicted in **Figures 8** and **S18–21**. For all advisory events, ResH2 and ResH4, i.e., woodsmoke, were the predominant contributors *before* and *after* the advisories were in place. A notable increase was observed in ResH3 contribution, i.e., heating oil, *during* the 2nd (Stage 1), 5th (Stage 1), 6th (Stage 1), and 7th advisory events. At the same time, ResH2 (i.e., hardwood-related fuels) remained a prominent contributor to OA_{CHARON} *during* the 3rd (Stage 2), 4th (Stage 1), and 5th (Stage 1) advisories. Most households in Fairbanks use heating oil (~72% of residents), followed by wood (~22% of residents) (Dunleavy and Brune, 2019), which was not reflected in the relative contributions apportioned to ResH3. This can be linked to a higher PM_1 release from wood combustion per given volume of fuel compared to heating oil and/or an underestimation of ResH3 by PTR_{CHARON} being associated with smaller than 100 nm (**Figure S12**).

As expected, the absolute average concentrations of all factors were inversely related to ambient temperature; however, the percent change differed considerably across factors. Specifically, as temperatures decreased from -10°C to below -25°C, the average absolute concentrations for $transport_{CHARON}$, COA_{CHARON}, OOA_{CHARON}, ResH1–4 increased 0.25×, 0.75×, 9.0×, 1.4×, 25.1×, 3.0×, and 2.9×, respectively (**Figure S22**). The steep increase in the relative contribution of ResH2, associated with hardwood tracers, contrasts with previous reports based on surveys (Dunleavy and Brune, 2019) and organic tracers (Haque et al., 2021), indicating birch and spruce as the most popular firewood in Fairbanks. Laboratory studies have shown that the burning of softwood pellets of Douglas Fir or eastern white pine emits less PM than hardwood pellets of the same volume, and this response varies based on the moisture content of the wood and the heating appliance used (Morin et al., 2022). Also, ResH2 comprises a broader spectrum of volatile and semi-volatile substituted phenolic species. Thus, it is likely to undergo efficient gas-to-particle partitioning at low temperatures, leading to increased OA loads (Ijaz et al., 2025).

5. Conclusion

A CHARON inlet coupled with PTR-ToF MS and HR-ToF AMS were deployed during the Alaskan Layered Pollution and Chemical Analysis (ALPACA) campaign. The PMF analysis of AMS data revealed three primary factors: biomass burning, hydrocarbon-like, and cooking factors, accounting for 28, 38, and 11% of the total OA, respectively. A combined organic and inorganic PMF analysis provided additional insights. It revealed the presence of organosulphur compounds mostly associated with the OOA factor and with another sulphate-rich factor of an acidic nature. A nitrate factor associated with hydrocarbon-like OA and high NO_x levels was interpreted as aged road transport emissions. The PTR_{CHARON} PMF analysis could differentiate between four residential heating sources—one oil combustion and three wood combustion types associated with low temperature and softwood or hardwood combustion. Such factorisation was achieved with the support of specific tracers that CHARON could successfully identify, as furans, aromatic alcohols (resorcinol, guaiacol, eugenol, syringol), aldehydes (furfural, coniferaldehyde), acids (benzoic, dehydroabietic, abietic, linoleic, oleic, and stearic) and various PAHs. Collectively, all residential heating factors accounted for 79% of the total OA_{CHARON}. Cooking and road transport were also recognised as primary sources by PTR_{CHARON}. All PMF analyses could apportion a single secondary organic fraction accounting for 11-19% of the total OA. This work demonstrates the complementarity of the two instruments and their ability to describe the complex chemical composition of PM_1 and its related sources. The enhanced deconvolution of closely co-varying sources of ambient pollution epitomises the novelty of our study. It demonstrates the capability of PTR_{CHARON} to deliver detailed qualitative and quantitative insights, thus enabling a

comprehensive understanding of organic aerosol sources. These advances can support environmental regulators and citizen efforts to improve air quality in Fairbanks and the fast-urbanising regional sub-Arctic areas.

Data availability

Supporting text, figures, and tables are available in the Supplementary Material.

Author contributions

The manuscript was written with the contributions of all authors. BT-R and BDA set up, ran, and maintained the instrumentation during the campaign in Fairbanks. SA, NB, and ED aided during the campaign. MC-S collected and contributed meteorological and trace gas data. BA, RJW, KD, and AM provided data on ion chromatography analysis of offline filter samples. BT-R and AI processed and analysed the data with help from BC. WS and KS coordinated the ALPACA and CASPA projects. KL, BDA, BB, SB, JF, JM, and JS contributed to funding acquisition for the CASPA project. BDA supervised the project reported here.

Competing interests

The authors declare that they have no conflict of interest.

Acknowledgements

We thank the ALPACA team of researchers and all others involved in designing the project and providing the necessary logistical support to carry it out. We thank Dr Anna Tobler (Datalystica Ltd, Switzerland) for providing technical support for SoFi analysis. This work was funded by the CASPA (Climate-relevant Aerosol Sources and Processes in the Arctic) project of the Agence Nationale de la Recherche (grant no. ANR-21-CE01-0017) and the IPEV (French Polar Institute Paul-Émile Victor). KD and RJW were supported by the National Science Foundation's (NSF) Atmospheric Geoscience Program (grant no. AGS-2029730) and the NSF Navigating the New Arctic Program (grant no. NNA-1927778). SRA acknowledges support from the UK Natural Environment Research Council (grant ref: NE/W00609X/1). We thank the MASSALYA instrumental platform (Aix-Marseille Université, Laboratory of Chemistry and Environment, lce.univ-amu.fr) for the measurements used in this

publication. AI is grateful to Subuktageen Qitta, Nastaran Mahmud, Laal Boo'on-Wali, and Minuit Mahmud for the many valuable discussions that helped compile this report.

References

Aiken, A. C., DeCarlo, P. F., and Jimenez, J. L.: Elemental analysis of organic species with electron ionization high-resolution mass spectrometry, Analytical chemistry, 79, 8350-8358, 2007.

Aiken, A. C., Decarlo, P. F., Kroll, J. H., Worsnop, D. R., Huffman, J. A., Docherty, K. S., Ulbrich, I. M., Mohr, C., Kimmel, J. R., and Sueper, D.: O/C and OM/OC ratios of primary, secondary, and ambient organic aerosols with high-resolution time-of-flight aerosol mass spectrometry, Environmental science & technology, 42, 4478-4485, 2008.

Alaska Department of Environmental Conservation, Know Your Wood: https://dec.alaska.gov/air/burnwise/know-your-wood

Alves, C. A., Vicente, E. D., Rocha, S., and Vicente, A. M.: Organic tracers in aerosols from the residential combustion of pellets and agro-fuels, Air Quality, Atmosphere & Health, 10, 37-45, 2017.

Bari, M. A., Baumbach, G., Kuch, B., and Scheffknecht, G.: Wood smoke as a source of particle-phase organic compounds in residential areas, Atmospheric Environment, 43, 4722–4732, 2009.

Brégonzio-Rozier, L., Siekmann, F., Giorio, C., Pangui, E., Morales, S., Temime-Roussel, B., Gratien, A., Michoud, V., Ravier, S., and Cazaunau, M.: Gaseous products and secondary organic aerosol formation during long term oxidation of isoprene and methacrolein, Atmospheric Chemistry and Physics, 15, 2953-2968, 2015.

Campbell, J. R., Battaglia Jr, M., Dingilian, K., Cesler-Maloney, M., St Clair, J. M., Hanisco, T. F., Robinson, E., DeCarlo, P., Simpson, W., and Nenes, A.: Source and Chemistry of Hydroxymethanesulfonate (HMS) in Fairbanks, Alaska, Environmental Science & Technology, 2022.

Campbell, J. R., Battaglia Jr, M., Dingilian, K. K., Cesler-Maloney, M., Simpson, W. R., Robinson, E. S., DeCarlo, P. F., Temime-Roussel, B., D'Anna, B., and Holen, A. L.: Enhanced aqueous formation and neutralization of fine atmospheric particles driven by extreme cold, Science Advances, 10, eado4373, 2024.

Canagaratna, M., Jayne, J., Jimenez, J., Allan, J., Alfarra, M., Zhang, Q., Onasch, T., Drewnick, F., Coe, H., and Middlebrook, A.: Chemical and microphysical characterization of ambient aerosols with the aerodyne aerosol mass spectrometer, Mass spectrometry reviews, 26, 185-222, 2007.

Canagaratna, M., Jimenez, J., Kroll, J., Chen, Q., Kessler, S., Massoli, P., Hildebrandt Ruiz, L., Fortner, E., Williams, L., and Wilson, K.: Elemental ratio measurements of organic compounds using aerosol mass spectrometry: characterization, improved calibration, and implications, Atmospheric Chemistry and Physics, 15, 253-272, 2015.

Canagaratna, M. R., Jayne, J. T., Ghertner, D. A., Herndon, S., Shi, Q., Jimenez, J. L., Silva, P. J., Williams, P., Lanni, T., and Drewnick, F.: Chase studies of particulate emissions from in-use New York City vehicles, Aerosol Science and Technology, 38, 555-573, 2004.

Canonaco, F., Crippa, M., Slowik, J. G., Baltensperger, U., and Prévôt, A. S.: SoFi, an IGOR-based interface for the efficient use of the generalized multilinear engine (ME-2) for the source apportionment: ME-2 application to aerosol mass spectrometer data, Atmospheric Measurement Techniques, 6, 3649-3661, 2013.

Cash, J. M., Langford, B., Di Marco, C., Mullinger, N., Allan, J., Reyes-Villegas, E., Joshi, R., Heal, M. R., Acton, W. J. F., and Hewitt, N.: Seasonal analysis of submicron aerosol in Old Delhi using high resolution aerosol mass spectrometry: Chemical characterisation, source apportionment and new marker identification, Atmospheric Chemistry and Physics Discussions, 2020, 1-42, 2020.

Cesler-Maloney, M., Simpson, W., Kuhn, J., Stutz, J., Thomas, J., Roberts, T., Huff, D., and Cooperdock, S.: Shallow boundary layer heights controlled by the surface-based temperature inversion strength are responsible for trapping home heating emissions near the ground level in Fairbanks, Alaska, EGUsphere, 2024, 1-51, 2024.

Cesler-Maloney, M., Simpson, W. R., Miles, T., Mao, J., Law, K. S., and Roberts, T. J.: Differences in Ozone and Particulate Matter Between Ground Level and 20 m Aloft are Frequent During Wintertime Surface-Based Temperature Inversions in Fairbanks, Alaska, Journal of Geophysical Research: Atmospheres, 127, e2021JD036215, 2022.

Chazeau, B., El Haddad, I., Canonaco, F., Temime-Roussel, B., d'Anna, B., Gille, G., Mesbah, B., Prévôt, A. S., Wortham, H., and Marchand, N.: Organic aerosol source apportionment by using rolling positive matrix factorization: Application to a Mediterranean coastal city, Atmospheric environment: X, 14, 100176, 2022.

Chen, G., Canonaco, F., Tobler, A., Aas, W., Alastuey, A., Allan, J., Atabakhsh, S., Aurela, M., Baltensperger, U., and Bougiatioti, A.: European aerosol phenomenology− 8: Harmonised source apportionment of organic aerosol using 22 Year-long ACSM/AMS datasets, Environment international, 166, 107325, 2022.

Chen, G., Li, S., Zhang, Y., Zhang, W., Li, D., Wei, X., He, Y., Bell, M. L., Williams, G., and Marks, G. B.: Effects of ambient PM1 air pollution on daily emergency hospital visits in China: an epidemiological study, The Lancet Planetary Health, 1, e221-e229, 2017.

Chen, Y., Xu, L., Humphry, T., Hettiyadura, A. P., Ovadnevaite, J., Huang, S., Poulain, L., Schroder, J. C., Campuzano-Jost, P., and Jimenez, J. L.: Response of the aerodyne aerosol mass spectrometer to inorganic sulfates and organosulfur compounds: Applications in field and laboratory measurements, Environmental science & technology, 53, 5176-5186, 2019.

Collard, F.-X. and Blin, J.: A review on pyrolysis of biomass constituents: Mechanisms and composition of the products obtained from the conversion of cellulose, hemicelluloses and lignin, Renew. Sustain. Energy Rev., 38, 594–608, https://doi.org/10.1016/j.rser.2014.06.013, 2014.

Crippa, M., Canonaco, F., Lanz, V., Äijälä, M., Allan, J., Carbone, S., Capes, G., Ceburnis, D., Dall'Osto, M., and Day, D.: Organic aerosol components derived from 25 AMS data sets across Europe using a consistent ME-2 based source apportionment approach, Atmospheric chemistry and physics, 14, 6159-6176, 2014.

Cubison, M., Ortega, A., Hayes, P., Farmer, D., Day, D., Lechner, M., Brune, W., Apel, E., Diskin, G., and Fisher, J.: Effects of aging on organic aerosol from open biomass burning smoke in aircraft and laboratory studies, Atmospheric Chemistry and Physics, 11, 12049-12064, 2011.

Czarnecki, N.: Local Air Quality Regulations: How to Participate and Comply, Clear the Air Home Heating Forum and Expo,

DeCarlo, P. F., Kimmel, J. R., Trimborn, A., Northway, M. J., Jayne, J. T., Aiken, A. C., Gonin, M., Fuhrer, K., Horvath, T., and Docherty, K. S.: Field-deployable, high-resolution, time-of-flight aerosol mass spectrometer, Analytical chemistry, 78, 8281-8289, 2006.

Dingilian, K., Hebert, E., Battaglia Jr, M., Campbell, J. R., Cesler-Maloney, M., Simpson, W., St. Clair, J. M., Dibb, J., Temime-Roussel, B., and D'anna, B.: Hydroxymethanesulfonate and Sulfur (IV) in Fairbanks Winter During the ALPACA Study, ACS ES&T Air, 2024.

Dunleavy, M. and Brune, J. W.: Amendments to: State Air Quality Control Plan. Vol. III: Appendix III.D.7.06, 2019.

Dunleavy, M. J. and Brune, J. W.: Amendments to State Air Quality Control Plan: Vol. III: Appendix III.D.7.7, Alaska Department of Environmental Conservation, 2020.

Eichler, P., Müller, M., D'anna, B., and Wisthaler, A.: A novel inlet system for online chemical analysis of semi-volatile submicron particulate matter, Atmospheric Measurement Techniques, 8, 1353-1360, 2015.

Eichler, P., Müller, M., Rohmann, C., Stengel, B., Orasche, J. r., Zimmermann, R., and Wisthaler, A.: Lubricating oil as a major constituent of ship exhaust particles, Environmental Science & Technology Letters, 4, 54-58, 2017.

Ellis, A. and Mayhew, C.: Chemical Ionization: Chemistry, Thermodynamics and Kinetics, Proton Transfer Reaction Mass Spectrometry, 25-48, 2014.

Fairbanks Air Quality Plan: https://www.epa.gov/ak/fairbanks-air-quality-plan, last access: May 07, 2024.
Fine, P. M., Cass, G. R., and Simoneit, B. R.: Chemical characterization of fine particle emissions from fireplace combustion of woods grown in the northeastern United States, Environmental Science & Technology, 35, 2665-2675, 2001.
Fine, P. M., Cass, G. R., and Simoneit, B. R.: Organic compounds in biomass smoke from residential wood combustion: Emissions characterization at a continental scale, Journal of Geophysical Research: Atmospheres, 107, ICC 11-11-ICC 11-19, 2002.
Fraser, M. P. and Lakshmanan, K.: Using levoglucosan as a molecular marker for the long-range transport of biomass combustion aerosols, Environmental Science & Technology, 34, 4560-4564, 2000.
Fye, M., Havel, B., Havel, H., and Putnam, J.: Opportunities for Air Quality Improvement in the Fairbanks North Star Borough, 2009.
Gkatzelis, G. I., Hohaus, T., Tillmann, R., Gensch, I., Müller, M., Eichler, P., Xu, K.-M., Schlag, P., Schmitt, S. H., and Yu, Z.: Gas-to-particle partitioning of major biogenic oxidation products: a study on freshly formed and aged biogenic SOA, Atmospheric chemistry and physics, 18, 12969-12989, 2018.
Glasius, M., Ketzel, M., Wåhlin, P., Jensen, B., Mønster, J., Berkowicz, R., and Palmgren, F.: Impact of wood combustion on particle levels in a residential area in Denmark, Atmospheric Environment, 40, 7115-7124, 2006.
Gueneron, M., Erickson, M. H., VanderSchelden, G. S., and Jobson, B. T.: PTR-MS fragmentation patterns of gasoline hydrocarbons, International Journal of Mass Spectrometry, 379, 97-109, 2015.
Guo, S., Hu, M., Peng, J., Wu, Z., Zamora, M. L., Shang, D., Du, Z., Zheng, J., Fang, X., and Tang, R.: Remarkable nucleation and growth of ultrafine particles from vehicular exhaust, Proceedings of the National Academy of Sciences, 117, 3427-3432, 2020.
Haque, M. M., Kawamura, K., Deshmukh, D. K., Kunwar, B., and Kim, Y.: Biomass burning is an important source of organic aerosols in interior Alaska, Journal of Geophysical Research: Atmospheres, 126, e2021JD034586, 2021.
Herring, C. L., Faiola, C. L., Massoli, P., Sueper, D., Erickson, M. H., McDonald, J. D., Simpson, C. D., Yost, M. G., Jobson, B. T., and VanReken, T. M.: New methodology for quantifying polycyclic aromatic hydrocarbons (PAHs) using high-resolution aerosol mass spectrometry, Aerosol Science and Technology, 49, 1131-1148, 2015.
Ijaz, A., Temime Roussel, B., Kammer, J., Mao, J., Simpson, W., Law, K., and D'Anna, B.: In situ measurements of gas-particle partitioning of organic compounds in Fairbanks, Faraday Discussions - In Prep, 2025.
Janhäll, S., Andreae, M. O., and Pöschl, U.: Biomass burning aerosol emissions from vegetation fires: particle number and mass emission factors and size distributions, Atmospheric chemistry and physics, 10, 1427-1439, 2010.
Jentgen, M.: Technical support document for Alaska Department of Environmental Conservation's (ADEC) control measure analysis, under 40 CFR 1010(a) and (c), US EPA, Region 10, Air and Radiation Division, 2022.
Jiang, X., Tsona, N. T., Jia, L., Liu, S., Zhang, H., Xu, Y., and Du, L.: Secondary organic aerosol formation from photooxidation of furan: effects of NO x and humidity, Atmospheric chemistry and physics, 19, 13591-13609, 2019.
Joyce, P., Von Glasow, R., and Simpson, W.: The fate of NO x emissions due to nocturnal oxidation at high latitudes: 1-D simulations and sensitivity experiments, Atmospheric Chemistry and Physics, 14, 7601-7616, 2014.
Katz, E. F., Guo, H., Campuzano-Jost, P., Day, D. A., Brown, W. L., Boedicker, E., Pothier, M., Lunderberg, D. M., Patel, S., and Patel, K.: Quantification of cooking organic aerosol in the indoor environment using aerodyne aerosol mass spectrometers, Aerosol Science and Technology, 55, 1099-1114, 2021.
Kawamoto, H.: Lignin pyrolysis reactions, Journal of Wood Science, 63, 117-132, 2017.
Kong, X., Salvador, C. M., Carlsson, S., Pathak, R., Davidsson, K. O., Le Breton, M., Gaita, S. M., Mitra, K., Hallquist, Å. M., and Hallquist, M.: Molecular characterization and optical properties of primary emissions from a residential wood burning boiler, Science of the Total Environment, 754, 142143, 2021.
Koss, A. R., Sekimoto, K., Gilman, J. B., Selimovic, V., Coggon, M. M., Zarzana, K. J., Yuan, B., Lerner, B. M., Brown, S. S., Jimenez, J. L., Krechmer, J., Roberts, J. M., Warneke, C., Yokelson, R. J., and De Gouw, J.: Non-methane organic gas

emissions from biomass burning: identification, quantification, and emission factors from PTR-ToF during the FIREX 2016 laboratory experiment, Atmospheric Chem. Phys., 18, 3299–3319, https://doi.org/10.5194/acp-18-3299-2018, 2018.
Kostenidou, E., Marques, B., Temime-Roussel, B., Liu, Y., Vansevenant, B., Sartelet, K., and D'Anna, B.: Secondary organic aerosol formed by Euro 5 gasoline vehicle emissions: chemical composition and gas-to-particle phase partitioning, Atmospheric Chemistry and Physics, 24, 2705-2729, 2024.
Kostenidou, E., Martinez-Valiente, A., R'Mili, B., Marques, B., Temime-Roussel, B., André, M., Liu, Y., Louis, C., Vansevenant, B., and Ferry, D.: Emission factors, chemical composition and morphology of particles emitted from Euro 5 diesel and gasoline light duty vehicles during transient cycles, Atmospheric Chemistry and Physics Discussions, 2020, 1-33, 2020.
Kotchenruther, R. A.: Source apportionment of PM2. 5 at multiple Northwest US sites: Assessing regional winter wood smoke impacts from residential wood combustion, Atmospheric Environment, 142, 210-219, 2016.
Kumar, V., Giannoukos, S., Haslett, S. L., Tong, Y., Singh, A., Bertrand, A., Lee, C. P., Wang, D. S., Bhattu, D., and Stefenelli, G.: Highly time-resolved chemical speciation and source apportionment of organic aerosol components in Delhi, India, using extractive electrospray ionization mass spectrometry, Atmospheric Chemistry and Physics, 22, 7739-7761, 2022.
Lannuque, V., d'Anna, B., Kostenidou, E., Couvidat, F., Martinez-Valiente, A., Eichler, P., Wisthaler, A., Müller, M., Temime-Roussel, B., and Valorso, R.: Gas–particle partitioning of toluene oxidation products: an experimental and modeling study, Atmospheric Chemistry and Physics, 23, 15537-15560, 2023.
Leglise, J., Müller, M., Piel, F., Otto, T., and Wisthaler, A.: Bulk Organic Aerosol Analysis by Proton-Transfer-Reaction Mass Spectrometry: An Improved Methodology for the Determination of Total Organic Mass, O: C and H: C Elemental Ratios, and the Average Molecular Formula, Analytical chemistry, 91, 12619-12624, 2019.
Lignell, H., Epstein, S. A., Marvin, M. R., Shemesh, D., Gerber, B., and Nizkorodov, S.: Experimental and theoretical study of aqueous cis-pinonic acid photolysis, The Journal of Physical Chemistry A, 117, 12930-12945, 2013.
Liu, L., Breitner, S., Schneider, A., Cyrys, J., Brüske, I., Franck, U., Schlink, U., Leitte, A. M., Herbarth, O., and Wiedensohler, A.: Size-fractioned particulate air pollution and cardiovascular emergency room visits in Beijing, China, Environmental research, 121, 52-63, 2013.
Lopez-Hilfiker, F., Mohr, C., Ehn, M., Rubach, F., Kleist, E., Wildt, J., Mentel, T. F., Lutz, A., Hallquist, M., and Worsnop, D.: A novel method for online analysis of gas and particle composition: description and evaluation of a Filter Inlet for Gases and AEROsols (FIGAERO), Atmospheric Measurement Techniques, 7, 983-1001, 2014.
Louis, C., Liu, Y., Martinet, S., D'Anna, B., Valiente, A. M., Boreave, A., R'Mili, B., Tassel, P., Perret, P., and Andre, M.: Dilution effects on ultrafine particle emissions from Euro 5 and Euro 6 diesel and gasoline vehicles, Atmospheric environment, 169, 80-88, 2017.
Mainka, A. and Zajusz-Zubek, E.: PM1 in ambient and indoor air—urban and rural areas in the Upper Silesian Region, Poland, Atmosphere, 10, 662, 2019.
Mayfield, J. A. and Fochesatto, G. J.: The layered structure of the winter atmospheric boundary layer in the interior of Alaska, Journal of Applied Meteorology and Climatology, 52, 953-973, 2013.
McLafferty, F. W. and Tureˇcek, F.: Interpretation of mass spectra, Mill Valley (Calif.) : University Science Books, 4th ed. edn., ISBN 0935702253, 1993.
Meng, X., Ma, Y., Chen, R., Zhou, Z., Chen, B., and Kan, H.: Size-fractionated particle number concentrations and daily mortality in a Chinese city, Environmental health perspectives, 121, 1174-1178, 2013.
Middlebrook, A. M., Bahreini, R., Jimenez, J. L., and Canagaratna, M. R.: Evaluation of composition-dependent collection efficiencies for the aerodyne aerosol mass spectrometer using field data, Aerosol Science and Technology, 46, 258-271, 2012.
Mohr, C., Huffman, J. A., Cubison, M. J., Aiken, A. C., Docherty, K. S., Kimmel, J. R., Ulbrich, I. M., Hannigan, M., and Jimenez, J. L.: Characterization of primary organic aerosol emissions from meat cooking, trash burning, and motor vehicles

with high-resolution aerosol mass spectrometry and comparison with ambient and chamber observations, Environmental Science & Technology, 43, 2443-2449, 2009.
Montoya-Aguilera, J., Horne, J. R., Hinks, M. L., Fleming, L. T., Perraud, V., Lin, P., Laskin, A., Laskin, J., Dabdub, D., and Nizkorodov, S. A.: Secondary organic aerosol from atmospheric photooxidation of indole, Atmospheric Chemistry and Physics, 17, 11605-11621, 2017.
Moon, A., Jongebloed, U., Dingilian, K. K., Schauer, A. J., Chan, Y.-C., Cesler-Maloney, M., Simpson, W. R., Weber, R. J., Tsiang, L., and Yazbeck, F.: Primary Sulfate Is the Dominant Source of Particulate Sulfate during Winter in Fairbanks, Alaska, ACS ES&T Air, 2023.
Morin, B., Allen, G., Marin, A., Rector, L., and Ahmadi, M.: Impacts of wood species and moisture content on emissions from residential wood heaters, Journal of the Air & Waste Management Association, 72, 647-661, 2022.
Müller, M., Leglise, J., Piel, F., and Wisthaler, A.: A CHARON PTR-ToF-MS study on the volatility of freshly formed biogenic SOA, Geophysical Research Abstracts,
Müller, M., Eichler, P., D'Anna, B., Tan, W., and Wisthaler, A.: Direct sampling and analysis of atmospheric particulate organic matter by proton-transfer-reaction mass spectrometry, Analytical chemistry, 89, 10889-10897, 2017.
Paatero, P.: Least squares formulation of robust non-negative factor analysis, Chemometrics and intelligent laboratory systems, 37, 23-35, 1997a.
Paatero, P.: A weighted non-negative least squares algorithm for three-way 'PARAFAC'factor analysis, Chemometrics and Intelligent Laboratory Systems, 38, 223-242, 1997b.
Paatero, P.: The multilinear engine—a table-driven, least squares program for solving multilinear problems, including the n-way parallel factor analysis model, Journal of Computational and Graphical Statistics, 8, 854-888, 1999.
Paatero, P. and Hopke, P. K.: Discarding or downweighting high-noise variables in factor analytic models, Analytica Chimica Acta, 490, 277-289, 2003.
Paatero, P. and Tapper, U.: Positive matrix factorization: A non-negative factor model with optimal utilization of error estimates of data values, Environmetrics, 5, 111-126, 1994.
Paatero, P., Eberly, S., Brown, S., and Norris, G.: Methods for estimating uncertainty in factor analytic solutions, Atmospheric Measurement Techniques, 7, 781-797, 2014.
Palm, B. B., Peng, Q., Fredrickson, C. D., Lee, B. H., Garofalo, L. A., Pothier, M. A., Kreidenweis, S. M., Farmer, D. K., Pokhrel, R. P., and Shen, Y.: Quantification of organic aerosol and brown carbon evolution in fresh wildfire plumes, Proceedings of the National Academy of Sciences, 117, 29469-29477, 2020.
Peng, Y., Wang, H., Gao, Y., Jing, S., Zhu, S., Huang, D., Hao, P., Lou, S., Cheng, T., and Huang, C.: Real-time measurement of phase partitioning of organic compounds using a proton-transfer-reaction time-of-flight mass spectrometer coupled to a CHARON inlet, Atmospheric Measurement Techniques, 16, 15-28, 2023.
Piel, F., Müller, M., Mikoviny, T., Pusede, S. E., and Wisthaler, A.: Airborne measurements of particulate organic matter by proton-transfer-reaction mass spectrometry (PTR-MS): a pilot study, Atmospheric Measurement Techniques, 12, 5947-5958, 2019.
Piel, F., Müller, M., Winkler, K., Skytte af Sätra, J., and Wisthaler, A.: Introducing the extended volatility range proton-transfer-reaction mass spectrometer (EVR PTR-MS), Atmospheric Meas. Tech., 14, 1355–1363, 2021.
Pikridas, M., Sciare, J., Freutel, F., Crumeyrolle, S., Von Der Weiden-Reinmüller, S., Borbon, A., Schwarzenboeck, A., Merkel, M., Crippa, M., and Kostenidou, E.: In situ formation and spatial variability of particle number concentration in a European megacity, Atmospheric Chemistry and Physics, 15, 10219-10237, 2015.
Qi, L., Chen, M., Stefenelli, G., Pospisilova, V., Tong, Y., Bertrand, A., Hueglin, C., Ge, X., Baltensperger, U., and Prévôt, A. S.: Organic aerosol source apportionment in Zurich using an extractive electrospray ionization time-of-flight mass spectrometer (EESI-TOF-MS)–Part 2: Biomass burning influences in winter, Atmospheric Chemistry and Physics, 19, 8037-8062, 2019.

Reemtsma, T.: Determination of molecular formulas of natural organic matter molecules by (ultra-) high-resolution mass spectrometry: status and needs, Journal of chromatography A, 1216, 3687-3701, 2009.
Reid, J., Koppmann, R., Eck, T., and Eleuterio, D.: A review of biomass burning emissions part II: intensive physical properties of biomass burning particles, Atmospheric chemistry and physics, 5, 799-825, 2005.
Robinson, E. S., Cesler-Maloney, M., Tan, X., Mao, J., Simpson, W., and DeCarlo, P. F.: Wintertime spatial patterns of particulate matter in Fairbanks, AK during ALPACA 2022, Environmental Science: Atmospheres, 3, 568-580, 2023.
Robinson, E. S., Battaglia Jr, M., Campbell, J. R., Cesler-Maloney, M., Simpson, W., Mao, J., Weber, R. J., and DeCarlo, P. F.: Multi-year, high-time resolution aerosol chemical composition and mass measurements from Fairbanks, Alaska, Environmental Science: Atmospheres, 2024.
Schauer, J. J. and Cass, G. R.: Source apportionment of wintertime gas-phase and particle-phase air pollutants using organic compounds as tracers, Environmental science & technology, 34, 1821-1832, 2000.
Schueneman, M. K., Nault, B. A., Campuzano-Jost, P., Jo, D. S., Day, D. A., Schroder, J. C., Palm, B. B., Hodzic, A., Dibb, J. E., and Jimenez, J. L.: Aerosol pH indicator and organosulfate detectability from aerosol mass spectrometry measurements, Atmospheric Measurement Techniques, 14, 2237-2260, 2021.
Simoneit, B. R.: A review of biomarker compounds as source indicators and tracers for air pollution, Environmental Science and Pollution Research, 6, 159-169, 1999.
Simoneit, B. R.: Biomass burning—a review of organic tracers for smoke from incomplete combustion, Applied Geochemistry, 17, 129-162, 2002.
Simpson, W., Law, K., Schmale, J., Pratt, K., Arnold, S., Mao, J., Alexander, B., Anenberg, S., Baklanov, A., Bell, D., Brown, S., Creamean, J., Boer, G. d., DeCarlo, P., Descari, S., Elleman, R., Flynn, J., and al, e.: Alaskan Layered Pollution And Chemical Analysis (ALPACA) White Paper, 2019.
Simpson, W. R., Mao, J., Fochesatto, G. J., Law, K. S., DeCarlo, P. F., Schmale, J., Pratt, K. A., Arnold, S. R., Stutz, J., Dibb, J. E., Creamean, J. M., Weber, R. J., Williams, B. J., Alexander, B., Hu, L., Yokelson, R. J., Shiraiwa, M., Decesari, S., Anastasio, C., D'Anna, B., Gilliam, R. C., Nenes, A., St. Clair, J. M., Trost, B., Flynn, J. H., Savarino, J., Conner, L. D., Kettle, N., Heeringa, K. M., Albertin, S., Baccarini, A., Barret, B., Battaglia, M. A., Bekki, S., Brado, T. J., Brett, N., Brus, D., Campbell, J. R., Cesler-Maloney, M., Cooperdock, S., Cysneiros De Carvalho, K., Delbarre, H., DeMott, P. J., Dennehy, C. J. S., Dieudonné, E., Dingilian, K. K., Donateo, A., Doulgeris, K. M., Edwards, K. C., Fahey, K., Fang, T., Guo, F., Heinlein, L. M. D., Holen, A. L., Huff, D., Ijaz, A., Johnson, S., Kapur, S., Ketcherside, D. T., Levin, E., Lill, E., Moon, A. R., Onishi, T., Pappaccogli, G., Perkins, R., Pohorsky, R., Raut, J.-C., Ravetta, F., Roberts, T., Robinson, E. S., Scoto, F., Selimovic, V., Sunday, M. O., Temime-Roussel, B., Tian, X., Wu, J., and Yang, Y.: Overview of the Alaskan Layered Pollution and Chemical Analysis (ALPACA) Field Experiment, ACS EST Air, 1, 200–222, https://doi.org/10.1021/acsestair.3c00076, 2024.
Smith, D. M., Cui, T., Fiddler, M. N., Pokhrel, R. P., Surratt, J. D., and Bililign, S.: Laboratory studies of fresh and aged biomass burning aerosol emitted from east African biomass fuels–Part 2: Chemical properties and characterization, Atmospheric Chemistry and Physics, 20, 10169-10191, 2020.
Smith, S. J., van Aardenne, J., Klimont, Z., Andres, R. J., Volke, A., and Delgado Arias, S.: Anthropogenic sulfur dioxide emissions: 1850–2005, Atmospheric Chemistry and Physics, 11, 1101-1116, 2011.
Song, S., Gao, M., Xu, W., Sun, Y., Worsnop, D. R., Jayne, J. T., Zhang, Y., Zhu, L., Li, M., Zhou, Z., Cheng, C., Lv, Y., Wang, Y., Peng, W., Xu, X., Lin, N., Wang, Y., Wang, S., Munger, J. W., Jacob, D. J., and McElroy, M. B.: Possible heterogeneous chemistry of hydroxymethanesulfonate (HMS) in northern China winter haze, Atmos. Chem. Phys., 19, 1357-1371, 10.5194/acp-19-1357-2019, 2019.
Stefenelli, G., Pospisilova, V., Lopez-Hilfiker, F. D., Daellenbach, K. R., Hüglin, C., Tong, Y., Baltensperger, U., Prévôt, A. S., and Slowik, J. G.: Organic aerosol source apportionment in Zurich using an extractive electrospray ionization time-of-

flight mass spectrometer (EESI-TOF-MS)–Part 1: Biogenic influences and day–night chemistry in summer, Atmospheric Chemistry and Physics, 19, 14825-14848, 2019a.
Stefenelli, G., Jiang, J., Bertrand, A., Bruns, E. A., Pieber, S. M., Baltensperger, U., Marchand, N., Aksoyoglu, S., Prévôt, A. S., and Slowik, J. G.: Secondary organic aerosol formation from smoldering and flaming combustion of biomass: a box model parametrization based on volatility basis set, Atmospheric Chemistry and Physics, 19, 11461-11484, 2019b.
Sueper, D.: Squirrel and Pika Error Estimates, 2014.
Sun, Y.-L., Zhang, Q., Schwab, J., Demerjian, K., Chen, W.-N., Bae, M.-S., Hung, H.-M., Hogrefe, O., Frank, B., and Rattigan, O.: Characterization of the sources and processes of organic and inorganic aerosols in New York city with a high-resolution time-of-flight aerosol mass apectrometer, Atmospheric Chemistry and Physics, 11, 1581-1602, 2011.
Temime Roussel, B., Cesler-Maloney, M., Chazeau, B., Ijaz, A., Brett, N., Law, K., Bekki, S., Mao, J., Ketcherside, D., Selimovic, V., Hu, L., Simpson, W. R., and D'Anna, B.: Concentrations and Sources of VOCs during wintertime urban pollution at Fairbanks, Alaska, December 01, 20222022: https://agu.confex.com/agu/fm22/meetingapp.cgi/Paper/1072876
Tobler, A. K., Skiba, A., Canonaco, F., Močnik, G., Rai, P., Chen, G., Bartyzel, J., Zimnoch, M., Styszko, K., and Nęcki, J.: Characterization of non-refractory (NR) PM 1 and source apportionment of organic aerosol in Kraków, Poland, Atmospheric chemistry and physics, 21, 14893-14906, 2021.
Tong, Y., Pospisilova, V., Qi, L., Duan, J., Gu, Y., Kumar, V., Rai, P., Stefenelli, G., Wang, L., and Wang, Y.: Quantification of solid fuel combustion and aqueous chemistry contributions to secondary organic aerosol during wintertime haze events in Beijing, Atmospheric Chemistry and Physics, 21, 9859-9886, 2021.
Tran, H. N. and Mölders, N.: Investigations on meteorological conditions for elevated PM2. 5 in Fairbanks, Alaska, Atmospheric Research, 99, 39-49, 2011.
Ulbrich, I., Canagaratna, M., Zhang, Q., Worsnop, D., and Jimenez, J.: Interpretation of organic components from Positive Matrix Factorization of aerosol mass spectrometric data, Atmospheric Chemistry and Physics, 9, 2891-2918, 2009.
Wang, Y. and Hopke, P. K.: Is Alaska truly the great escape from air pollution?-long term source apportionment of fine particulate matter in Fairbanks, Alaska, Aerosol and Air Quality Research, 14, 1875-1882, 2014.
Wang, Y., Zhang, X., Sun, J., Zhang, X., Che, H., and Li, Y.: Spatial and temporal variations of the concentrations of PM 10, PM 2.5 and PM 1 in China, Atmospheric Chemistry and Physics, 15, 13585-13598, 2015.
Ward, T., Trost, B., Conner, J., Flanagan, J., and Jayanty, R.: Source apportionment of PM2. 5 in a subarctic airshed-fairbanks, Alaska, Aerosol and Air Quality Research, 12, 536-543, 2012.
Williams, B. J., Goldstein, A. H., Kreisberg, N. M., and Hering, S. V.: An in-situ instrument for speciated organic composition of atmospheric aerosols: T hermal desorption a erosol GC/MS-FID (TAG), Aerosol Science and Technology, 40, 627-638, 2006.
Xu, W., Li, Z., Zhang, Z., Li, J., Karnezi, E., Lambe, A. T., Zhou, W., Sun, J., Du, A., and Li, Y.: Changes in physicochemical properties of organic aerosol during photochemical aging of cooking and burning emissions, Journal of Geophysical Research: Atmospheres, 128, e2022JD037911, 2023.
Yang, Y., Battaglia, M. A., Mohan, M. K., Robinson, E. S., DeCarlo, P. F., Edwards, K. C., Fang, T., Kapur, S., Shiraiwa, M., and Cesler-Maloney, M.: Assessing the Oxidative Potential of Outdoor PM2. 5 in Wintertime Fairbanks, Alaska, ACS ES&T Air, 2024.
Ye, L. and Wang, Y.: Long-term air quality study in Fairbanks, Alaska: Air pollutant temporal variations, correlations, and PM2. 5 source apportionment, Atmosphere, 11, 1203, 2020.
Zhang, Q., Jimenez, J. L., Canagaratna, M. R., Ulbrich, I. M., Ng, N. L., Worsnop, D. R., and Sun, Y.: Understanding atmospheric organic aerosols via factor analysis of aerosol mass spectrometry: a review, Analytical and bioanalytical chemistry, 401, 3045-3067, 2011.

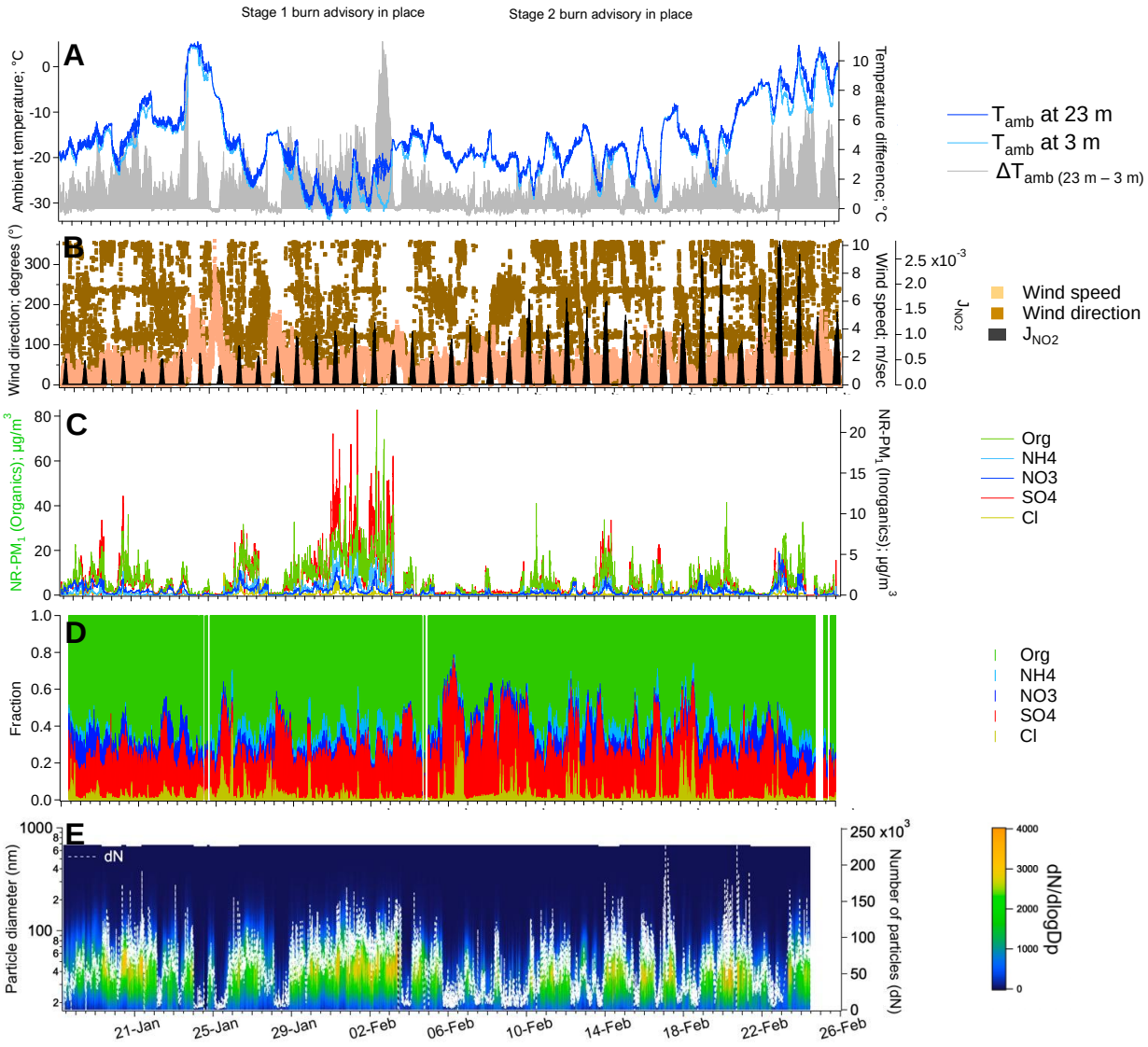

Figure 1. Overview of meteorological parameters and aerosol properties. The shaded areas indicate the periods when Stage 1 (red) and Stage 2 (black) advisories ("burn bans") from the Alaska Department of Environmental Conservation were in place in Fairbanks. (**A**) Ambient temperature at 3 and 23 m and difference of temperature between the two heights; (**B**) wind speed and direction with the daily sunlight in terms of the NO_2 photolysis rate coefficient (J_{NO2}) (Simpson et al., 2024) (**C**–**D**) absolute and fractional compositions of composition of non-refractory fine particulate matter (NR-PM_1) from the AMS; and (**E**) size distribution of PM_1 from the SMPS.

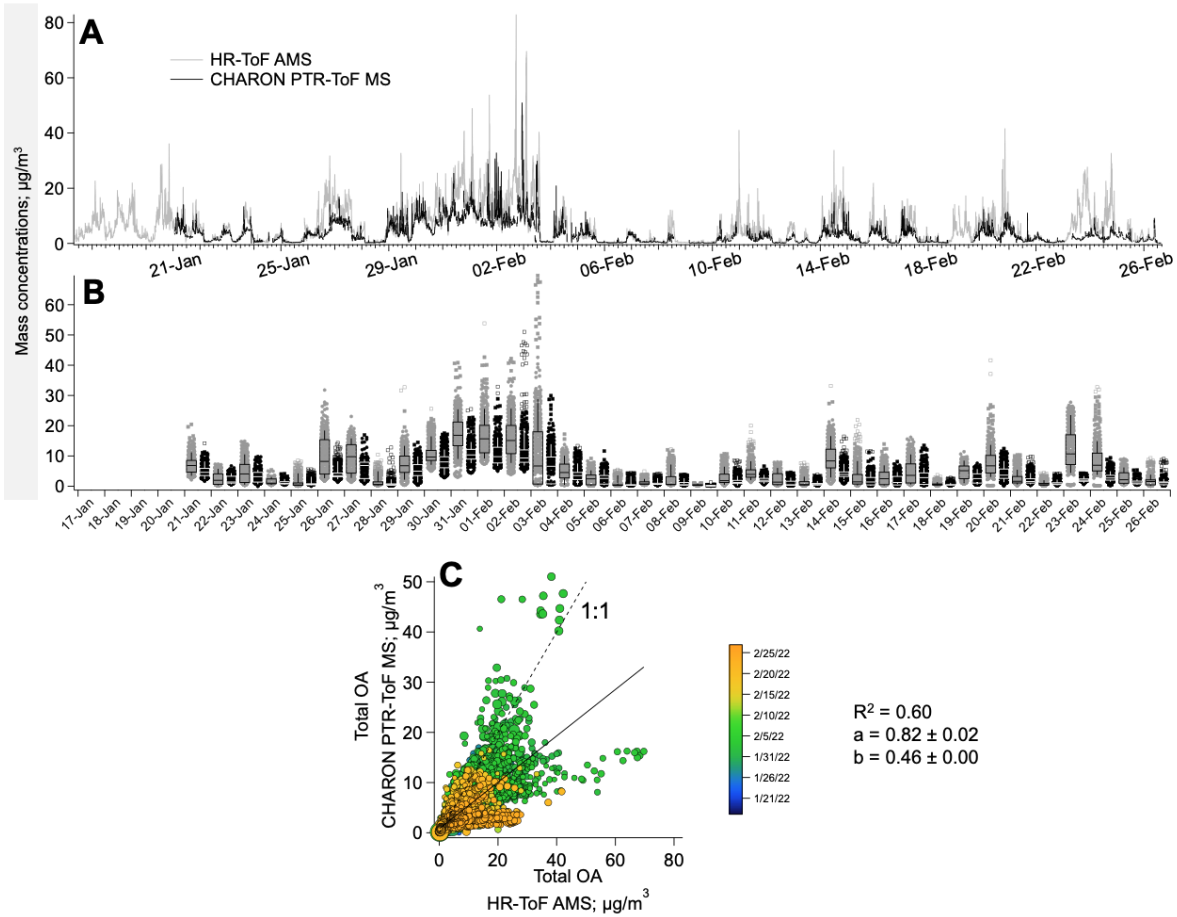

Figure 2. Comparison of total OA measured with the PTR_{CHARON} and the AMS. (**A**) Absolute concentrations of OA measured with the AMS and OA_{corr} (fragmentation-corrected OA) from PTR_{CHARON}; (**B**) Daily average concentrations of OA; and (**C**) Scatter plot of total OA measured with the AMS and the PTR_{CHARON}. Data points are coloured by the dates, and the legend is written as MM/DD/YY. Data points are sized by the geometric mean mass of the dM/dlogDp from SMPS (50–500 nm). The dashed line denotes the 1:1 relationship. Coefficients, *a* and *b*, denote the slope and the intercept for the linear regression ($p \leq 0.05$; solid line) and are written with ± one standard deviation.

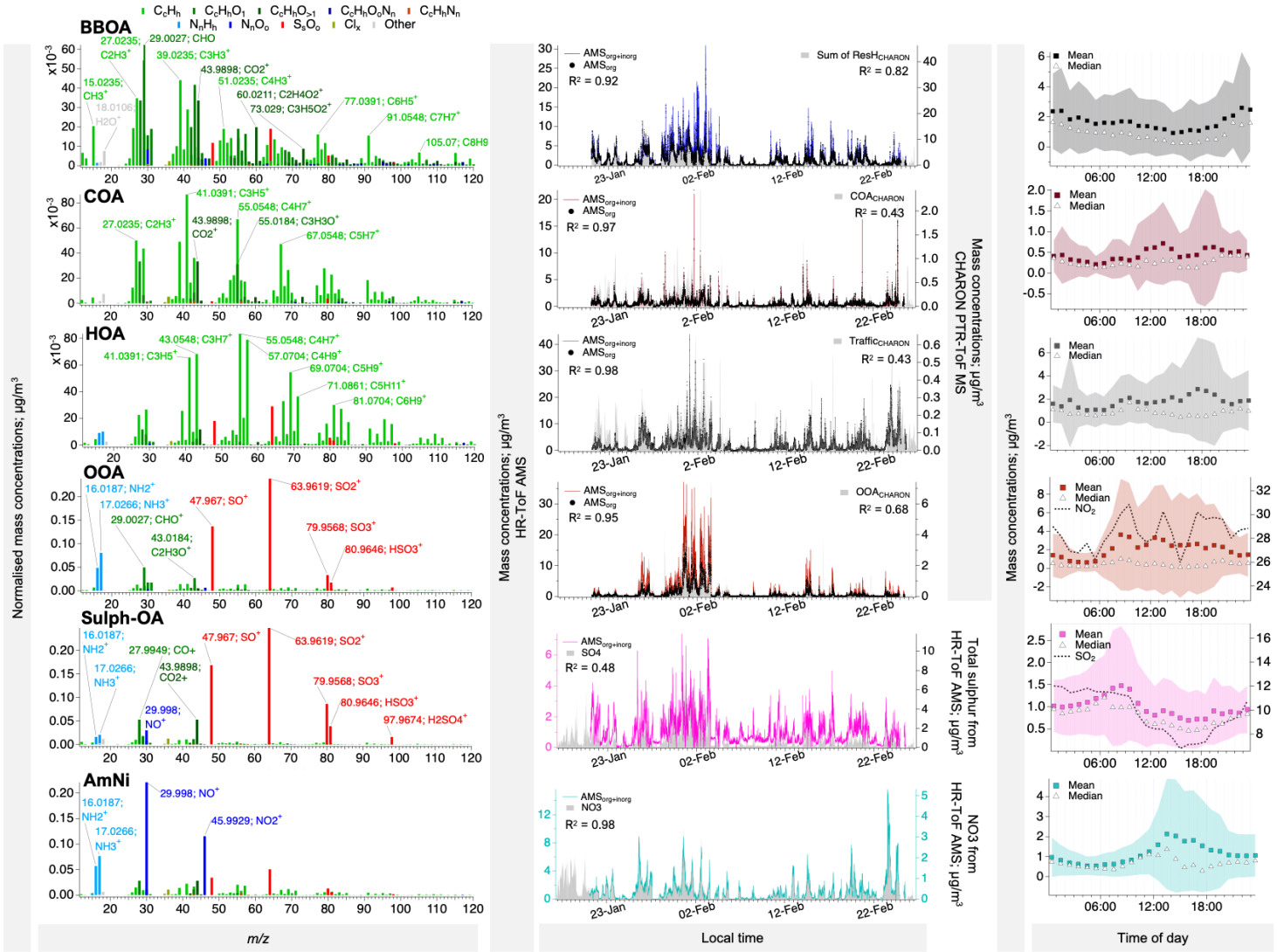

Figure 3. Overview of the positive matrix factorisation output for NR-PM_1 measurements with the $AMS_{org+inorg}$. Mass concentrations were normalised to the sum of the concentrations of all ions. Time series are overlaid with those of the corresponding factor (if available) in AMS_{org} and PTR_{CHARON} analysis or an external tracer. Correlation coefficients (R^2; $p \leq 0.05$) are also provided, and slopes can be found in **Table S5** or **Table 1**.

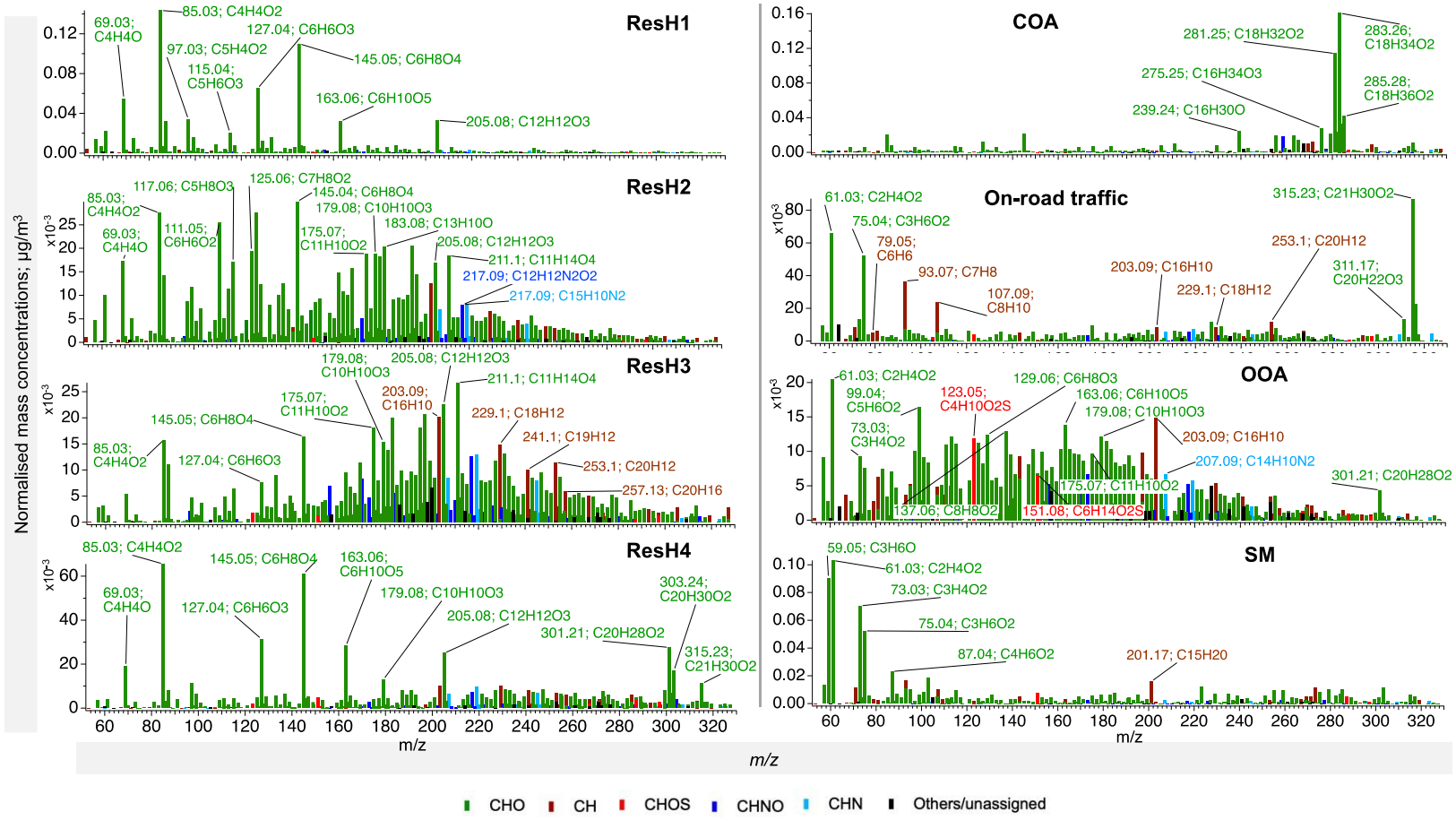

Figure 4. Normalised mass spectra of factors from the PMF of PTR_{CHARON} measurements. Mass concentrations are normalised to the sum of concentrations of all ions. Peaks are coloured by the molecular group (CHO, CHNO, CHOS, CH, CHN) of the formula assigned. Unassigned species are shown in black. Further information, such as tentative identities and formula errors, can be found in **Supplementary Dataset 1**.

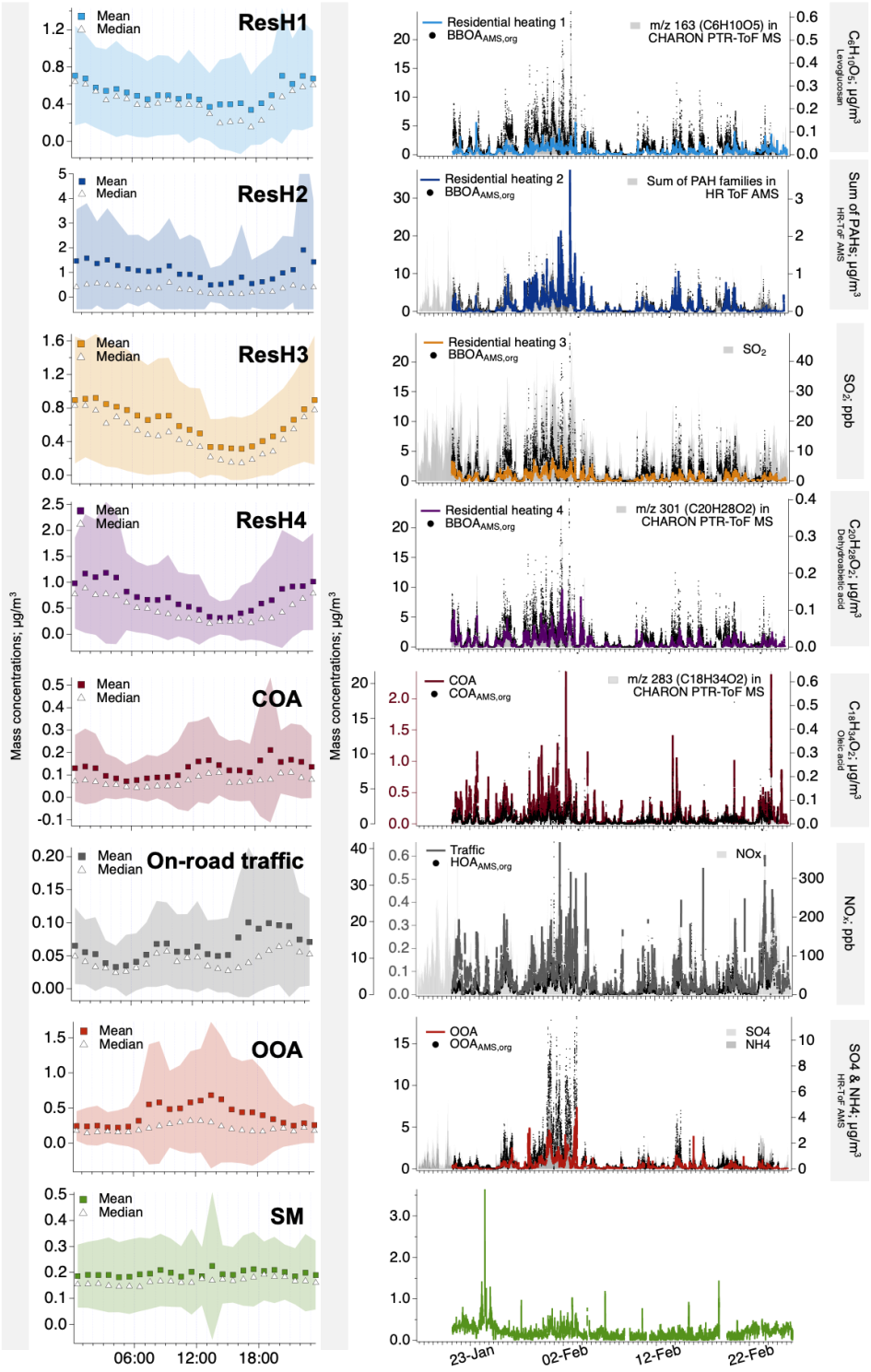

Figure 5. Diurnal profiles and complete time series of factors from the positive matrix factorisation of PTR_{CHARON} measurements. In the second column, time series are overlaid on those of the corresponding

factor in AMS_{org} and an external tracer or marker ion. Correlation coefficients (R^2; $p \leq 0.05$) are also provided, and slopes can be found in **Table S4** or **Table 1**.

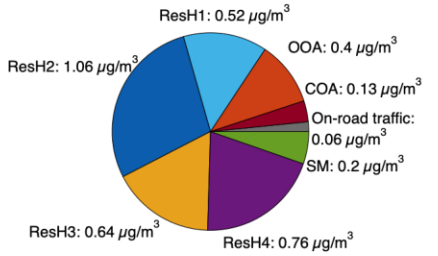

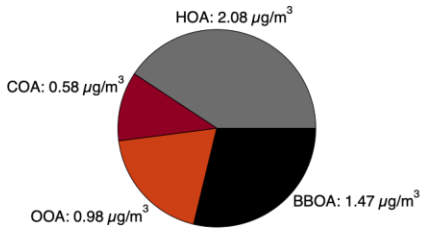

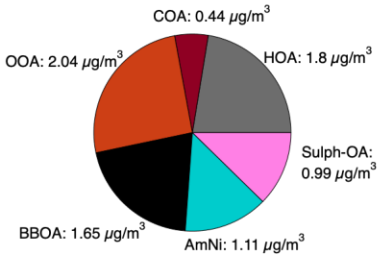

A	Mean mass concentration; μg/m³	Standard deviation	Maximum mass concentration; μg/m³
Total measured	3.41	3.84	51.04
Total modelled	3.35	3.77	48.01
Residential heating 1 (ResH1)	0.52	0.49	5.69
Residential heating 2 (ResH2)	1.06	1.88	37.56
Residential heating 3 (ResH3)	0.64	0.64	6.07
Residential heating 4 (ResH4)	0.76	0.90	9.73
Cooking (COA)	0.13	0.16	2.44
On-road traffic	0.06	0.07	0.66
Oxygenated OA (OOA)	0.40	0.60	7.43
Small molecules (SM)	0.20	0.14	3.64

B	Mean mass concentration; μg/m³	Standard deviation	Maximum mass concentration; μg/m³
Total measured	5.68	6.39	82.94
Total modelled	4.98	5.74	51.65
Biomass burning OA (BBOA)	1.47	1.93	24.85
Cooking (COA)	0.58	0.81	21.73
Hydrocarbon-like OA (HOA)	2.08	2.98	41.81
Oxygenated OA (OOA)	0.98	2.05	18.24

C	Mean mass concentration; μg/m³	Standard deviation	Maximum mass concentration; μg/m³
Total measured	8.31	9.29	92.66
Total modelled	7.57	8.74	67.66
Biomass burning OA (BBOA)	1.64	2.21	30.94
Cooking (COA)	0.44	0.72	21.05
Hydrocarbon-like OA (HOA)	1.80	2.71	43.85
Oxygenated OA (OOA)	2.04	4.14	37.18
Sulphate-rich (Sulph-OA)	0.99	0.83	7.39
Ammonium nitrate (AmNi)	1.12	1.59	15.63

Figure 6. Campaign-averages of mass concentrations apportioned to each factor in (**A**) PTR_{CHARON}, (**B**) AMS_{org}, and (**C**) $AMS_{org+inorg}$ analyses. Slices of pies are equivalent to the average absolute concentrations. A complete time series of fractional contributions can be found in **Figure S14**.

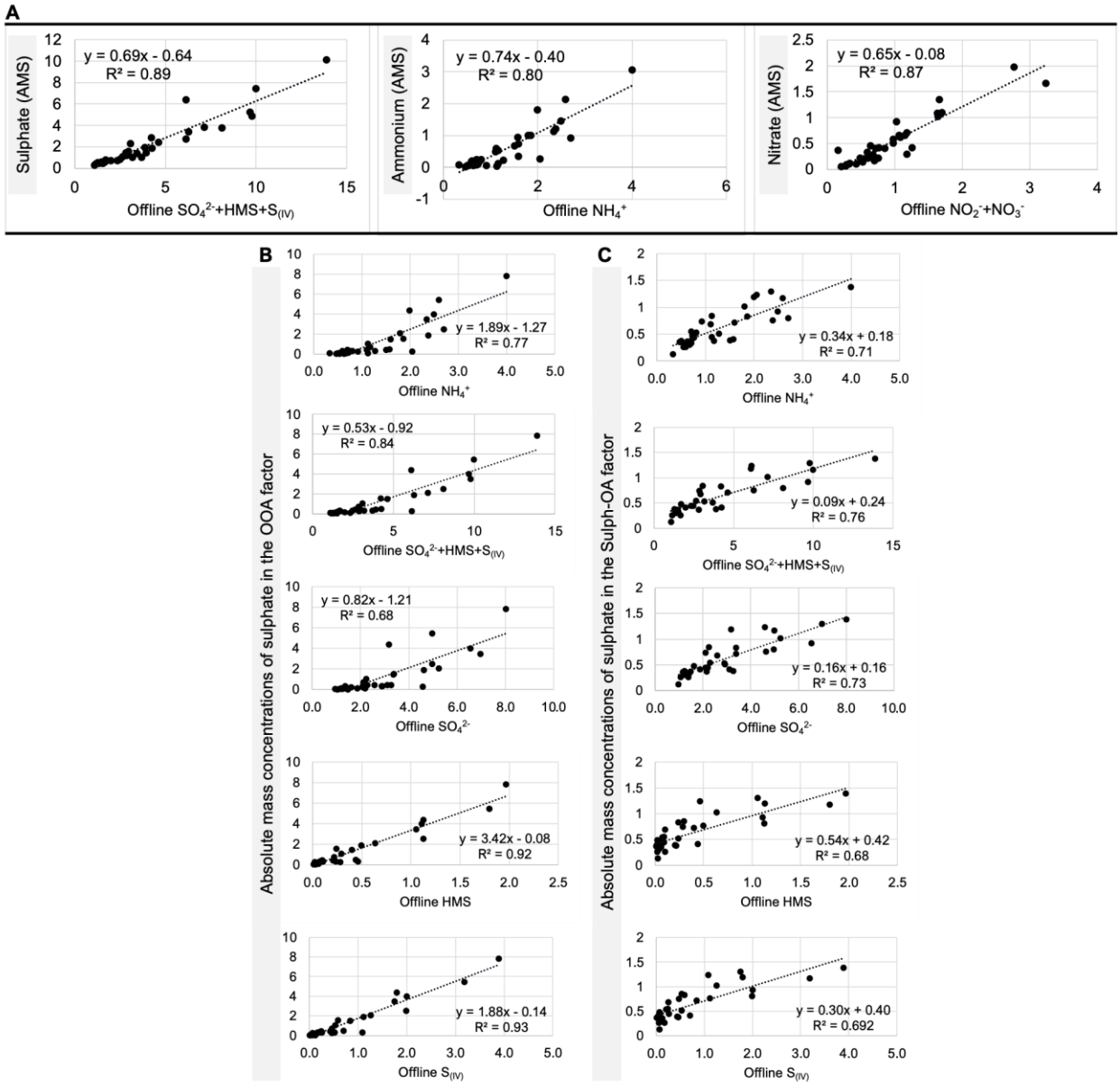

Figure 7. Scatter plots showing the correlation (R^2; $p \leq 0.05$) between inorganic species measured with the AMS and offline ion chromatography of chemical species in $PM_{0.7}$ collected on filters. Comparison of (**A**) total mass concentrations of sulphur and nitrogen-containing species; (B) $OOA_{AMS,org+inorg}$ factor with different species from IC analysis; and (**C**) Sulph-OA factor with different species from IC analysis.

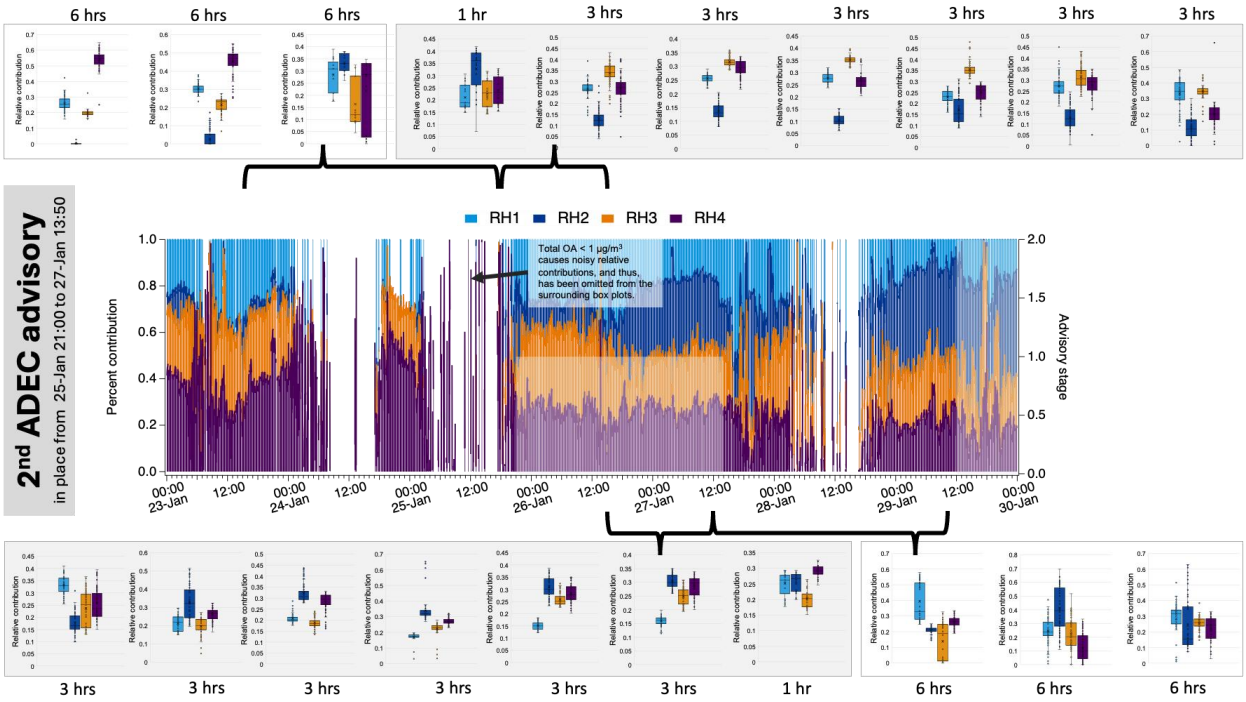

Figure 8. Variation in the relative contributions of residential heating factors to total biomass-burning OA concentrations. For simplicity, only the 2nd ADEC advisory implemented during the campaign is shown. Contributions are also shown for approximately 2 days before and after the advisory for comparison, along with their 6-hour averages as box plots (white panels), when suitable data was available (e.g., periods with noisy data were omitted and the adjacent period is shown instead). For better visualisation of variation in contributions, when the advisory was in place, 3-hour averages are shown (grey panels). To account for a lag in the appearance of variations in emission sources, 1-hour averages are shown for the beginning and end of the advisory event.

Table 1. Linear regression (R^2; $p \leq 0.05$) between the time series of factors derived from (**A**) PTR_{CHARON}, (**B**) AMS_{org}, and (**C**) $AMS_{org+inorg}$ measurements with external tracers and chemical species (S and N-containing species and PAHs) measured with the AMS.

A

	Traffic	COA	OOA	ResH1	ResH2	ResH3	ResH4	SM
Amb. Temp.	0.01	0.02	0.22	0.14	0.27	0.27	0.20	0.16
Black carbon	0.58	0.27	0.22	0.37	0.16	0.27	0.22	0.04
Trace gases								
NO_2	0.46	0.19	0.26	0.37	0.15	0.27	0.16	0.01
NO	0.65	0.24	0.22	0.32	0.10	0.16	0.13	0.06
NO_x	0.66	0.25	0.25	0.36	0.12	0.20	0.15	0.05
CO_2	0.67	0.38	0.31	0.51	0.24	0.39	0.30	0.02
CO	0.61	0.18	0.08	0.14	0.02	0.04	0.03	0.08
SO_2	0.27	0.20	0.19	0.46	0.34	0.61	0.47	0.01
O_3	0.34	0.19	0.13	0.39	0.12	0.31	0.20	0.00
Chemical species measured with the HR-ToF AMS								
Sulphur	0.43	0.22	0.71	0.35	0.22	0.23	0.13	0.04
NO_3	0.31	0.16	0.25	0.17	0.02	0.04	0.01	0.02
NH_4	0.43	0.20	0.64	0.30	0.15	0.14	0.06	0.05
Cl	0.10	0.05	0.12	0.06	0.01	0.03	0.01	0.01
UnSub PAH	0.30	0.25	0.34	0.50	0.59	0.55	0.58	0.01
M-PAH	0.33	0.27	0.33	0.52	0.60	0.53	0.60	0.01
O-PAH	0.27	0.22	0.36	0.56	0.70	0.61	0.64	0.01
N-PAH	0.28	0.23	0.26	0.54	0.62	0.61	0.68	0.01
A-PAH	0.28	0.24	0.19	0.48	0.50	0.55	0.61	0.04

B

	HOA	COA	OOA	BBOA
Amb. Temp.	0.02	0.02	0.19	0.22
Black carbon	0.49	0.27	0.29	0.25
Trace gases				
NO_2	0.42	0.25	0.25	0.25
NO	0.61	0.26	0.33	0.16
NO_x	0.62	0.28	0.34	0.20
CO_2	0.49	0.30	0.41	0.35
CO	0.38	0.19	0.19	0.06
SO_2	0.18	0.14	0.25	0.44
O_3	0.26	0.20	0.12	0.27
Chemical species measured with the HR-ToF AMS				
Sulphur	0.37	0.27	0.89	0.19
NO_3	0.49	0.27	0.23	0.06
NH_4	0.48	0.29	0.79	0.13
Cl	0.12	0.06	0.13	0.03
UnSub PAH	0.31	0.26	0.39	0.71
M-PAH	0.36	0.30	0.39	0.76
O-PAH	0.23	0.23	0.43	0.79
N-PAH	0.24	0.22	0.33	0.78
A-PAH	0.23	0.20	0.26	0.69

Very strong	≥0.75
Strong	≥0.5 and <0.75
Moderate	≥0.3 and <0.5
Weak	≥0.1 and <0.3
None	<0.1

C

	HOA	COA	OOA	BBOA	AmNi	Sulph-OA
Amb. Temp.	0.01	0.03	0.19	0.26	0.00	0.24
Black carbon	0.43	0.21	0.32	0.30	0.30	0.30
Trace gases						
NO_2	0.37	0.18	0.27	0.28	0.31	0.40
NO	0.55	0.19	0.36	0.22	0.35	0.32
NO_x	0.56	0.21	0.37	0.26	0.38	0.37
CO_2	0.41	0.24	0.47	0.41	0.28	0.48
CO	0.35	0.17	0.21	0.08	0.25	0.11
SO_2	0.14	0.11	0.27	0.45	0.07	0.61
O_3	0.23	0.14	0.12	0.25	0.23	0.34
Chemical species measured with the HR-ToF AMS						
Sulphur	0.26	0.24	0.95	0.34	0.23	0.48
NO_3	0.38	0.18	0.24	0.09	0.98	0.12
NH_4	0.34	0.25	0.86	0.25	0.44	0.33
Cl	0.09	0.05	0.15	0.04	0.16	0.04
UnSub PAH	0.26	0.25	0.40	0.77	0.15	0.31
M-PAH	0.31	0.28	0.40	0.82	0.17	0.32
O-PAH	0.18	0.23	0.41	0.87	0.11	0.33
N-PAH	0.20	0.20	0.33	0.82	0.11	0.30
A-PAH	0.20	0.18	0.26	0.70	0.11	0.25